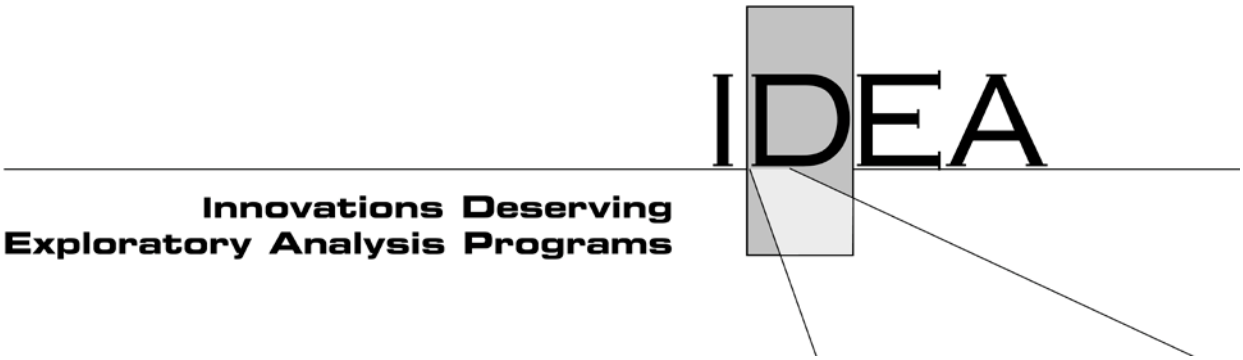

NCHRP IDEA Program

Enhanced Performance Zinc Coating for Steel in Concrete

Final Report for
NCHRP IDEA Project 174

Prepared by:
Neal S. Berke, Ph.D.
Tourney Consulting Group, LLC

November 2016

TRB TRANSPORTATION RESEARCH BOARD
The National Academies of
SCIENCES · ENGINEERING · MEDICINE

Innovations Deserving Exploratory Analysis (IDEA) Programs Managed by the Transportation Research Board

This IDEA project was funded by the NCHRP IDEA Program.

The TRB currently manages the following three IDEA programs:

- The NCHRP IDEA Program, which focuses on advances in the design, construction, and maintenance of highway systems, is funded by American Association of State Highway and Transportation Officials (AASHTO) as part of the National Cooperative Highway Research Program (NCHRP).
- The Safety IDEA Program currently focuses on innovative approaches for improving railroad safety or performance. The program is currently funded by the Federal Railroad Administration (FRA). The program was previously jointly funded by the Federal Motor Carrier Safety Administration (FMCSA) and the FRA.
- The Transit IDEA Program, which supports development and testing of innovative concepts and methods for advancing transit practice, is funded by the Federal Transit Administration (FTA) as part of the Transit Cooperative Research Program (TCRP).

Management of the three IDEA programs is coordinated to promote the development and testing of innovative concepts, methods, and technologies.

For information on the IDEA programs, check the IDEA website (www.trb.org/idea). For questions, contact the IDEA programs office by telephone at (202) 334-3310.

IDEA Programs
Transportation Research Board
500 Fifth Street, NW
Washington, DC 20001

The project that is the subject of this contractor-authored report was a part of the Innovations Deserving Exploratory Analysis (IDEA) Programs, which are managed by the Transportation Research Board (TRB) with the approval of the National Academies of Sciences, Engineering, and Medicine. The members of the oversight committee that monitored the project and reviewed the report were chosen for their special competencies and with regard for appropriate balance. The views expressed in this report are those of the contractor who conducted the investigation documented in this report and do not necessarily reflect those of the Transportation Research Board; the National Academies of Sciences, Engineering, and Medicine; or the sponsors of the IDEA Programs.

The Transportation Research Board; the National Academies of Sciences, Engineering, and Medicine; and the organizations that sponsor the IDEA Programs do not endorse products or manufacturers. Trade or manufacturers' names appear herein solely because they are considered essential to the object of the investigation.

Enhanced Performance Zinc Coating for Steel in Concrete

IDEA Program Final Report

Contract Number: NCHRP-174

Prepared for the IDEA Program

Transportation Research Board

The National Academics

Neal S. Berke, Ph.D.

Tourney Consulting Group, LLC

November 4, 2016

NCHRP IDEA PROGRAM COMMITTEE

CHAIR
DUANE BRAUTIGAM
Consultant

MEMBERS
CAMILLE CRICHTON-SUMNERS
New Jersey DOT
AGELIKI ELEFTERIADOU
University of Florida
ANNE ELLIS
Arizona DOT
ALLISON HARDT
Maryland State Highway Administration
JOE HORTON
California DOT
MAGDY MIKHAIL
Texas DOT
TOMMY NANTUNG
Indiana DOT
MARTIN PIETRUCHA
Pennsylvania State University
VALERIE SHUMAN
Shuman Consulting Group LLC
L.DAVID SUITS
North American Geosynthetics Society
JOYCE TAYLOR
Maine DOT

FHWA LIAISON
DAVID KUEHN
Federal Highway Administration

TRB LIAISON
RICHARD CUNARD
Transportation Research Board

COOPERATIVE RESEARCH PROGRAM STAFF
STEPHEN PARKER
Senior Program Officer

IDEA PROGRAMS STAFF
STEPHEN R. GODWIN
Director for Studies and Special Programs
JON M. WILLIAMS
Program Director, IDEA and Synthesis Studies
INAM JAWED
Senior Program Officer
DEMISHA WILLIAMS
Senior Program Assistant

EXPERT REVIEW PANEL

MARIO PAREDEDS, *Florida DOT*
RAY BOTTENBERG, *Oregon DOT*
MIKE BROWN, *Georgia DOT*
MIKE DALLAIRE, *FHWA*
TED HOPWOOD, *Kentucky Trans. Research Center*
STEVE KAHL, *Michigan DOT*
DARYL LITTLE, *US Bureau of Reclamation*

ACKNOWLEDGMENTS

We wish to acknowledge the following people and organizations that helped on this project:

Our review committee:

- Mario Paredes, Chairman—TRI Environmental (Florida DOT)
- Ray Bottenberg—Oregon DOT
- Mike Brown—Virginia Transportation Research Center
- Mike Dallaire—FHWA, Eastern Lands
- Ted Hopwood—Kentucky Transportation Research Center
- Steve Kahl—Michigan DOT
- Daryl Little—U.S. Bureau of Reclamation

The NCHRP for funding this work and our liaison Dr. Inam Jawed, Distek NA for additional funding and support, and the technicians and engineers at Tourney Consulting Group who assisted on this project. We wish to also acknowledge the contributions of Dr. Adam Rudy, who played a key role at the start of the project.

TABLE OF CONTENTS

1 EXECUTIVE SUMMARY 1

2 KEY FINDINGS AND SIGNIFICANT RESULTS 2

1 IDEA PRODUCT 3

1.1 INTRODUCTION 3

1.2 PRODUCT 3

1.3 POTENTIAL IMPACT ON TRANSPORTATION PRACTICE 3

2 CONCEPT AND INNOVATION 3

3 INVESTIGATION 4

3.1 MATERIAL TESTED 4

3.2 EXPERIMENTAL PROGRAM 6

3.2.1 Concrete Properties 6

3.2.2 Description of Tests 9

3.3 RESULTS AND DISCUSSIONS 12

3.3.1 Cracked Minibeams 12

3.3.2 U-Bends 36

4 PLANS FOR IMPLEMENTATION 43

5 CONCLUSIONS 44

6 INVESTIGATOR PROFILES 45

7 GLOSSARY AND REFERENCES 45

7.1 GLOSSARY 45

7.2 REFERENCES 45

APPENDIX A 47

A1 COMPOSITION OF STEEL USED 47

A2 REINFORCING BARS 48

1 EXECUTIVE SUMMARY

Emphasis on the long-term performance of bridges and other department of transportation (DOT) structures exposed to deicing or marine salts requires improving the corrosion resistance of embedded steel as well as the performance of the concrete. Stainless steel reinforcing bars are currently being specified in these structures, but with reduced permeability in the concrete, more cost-effective alternatives are attractive. Concerns with these alternatives are typically about corrosion at cracks in concrete as well as damage to the coating if coated steel is utilized.

This report evaluates thermal zinc diffusion (TZD) coatings on reinforcing bars, which provide the alloy bond found in hot-dipped galvanized (HDG) coatings with several advantages: a) tighter thickness tolerances, b) better ductility, c) applicability to high tensile strength steels, and d) less likelihood of embrittling the steel substrate. These coatings (ASTM A1059) have corrosion performance surpassing that of HDG, but uses so far have been for fasteners and other hardware in atmospheric and marine exposures.

Figure ES 1 shows the HDG versus the TZD bars. The TZD coating is a zinc-iron alloy versus the mostly zinc coating with HDG. The coating is more uniform for TZD bars.

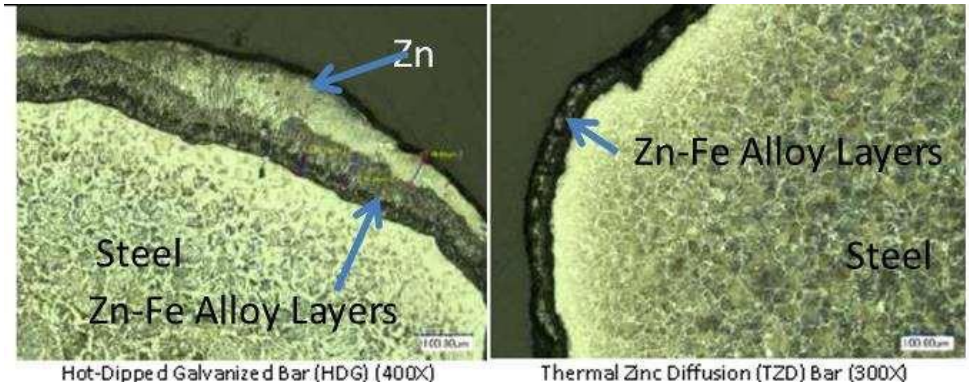

Figure ES 1 The HDG versus the TZD bars.

One benefit of the program is the development of an accelerated test method that is applicable to high-quality concrete. This study determined corrosion performance in good quality concrete cracked in flexure with periodic loading to abrade the coatings, to capture the two predominant failure mechanisms for coated steels. Both straight and bent bars were evaluated as well as another set of U-bend specimens for stress corrosion. Steels evaluated were black steel, HDG, epoxy-coated steel, 2304 Stainless Steel (SS), low chromium ASTM 1035 steel, and the TZD. An epoxy coating was manually applied to the TZD bars to evaluate a coated version of the product (TZE). Figure ES 2 shows the beam specimens and a schematic of a U-bend specimen.

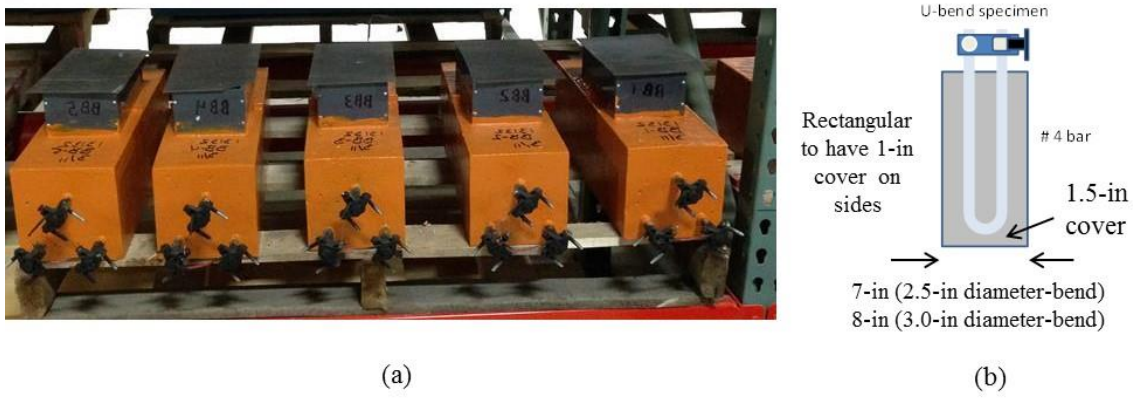

FIGURE ES 2 Cracked beam specimens (a) and schematic of U-bend specimen (b).

2 KEY FINDINGS AND SIGNIFICANT RESULTS

The performance of the corrosion-resistant reinforcing bars was significantly better than the control black bars. Extension of testing to two years made it easier to differentiate performance between the bars. The performance of reinforcements in the two test methods was different. This is somewhat due to the very quick ingress of chlorides in the U-bend specimens to all of the bar area, due to low cover and a higher water-to-cement ratio (w/c) = 0.5, whereas, even though the minibeams were cracked, the reinforcing bars were pulling the crack closed near the bar and cover was higher, so total chloride ingress was slower. Analysis of the chloride data showed that at the reinforcing bar level in the cracked concrete with 0.4 w/c and higher cover, the chloride levels were equivalent or lower than those in the U-bends. The overall relative corrosion resistance rankings in the cracked beam test were:

Black bar < HDG < A1035 low chromium < TZE ≈ TZD < ECR, 2304 SS

This supports the basis of the project that TZD reinforcing steel could improve the corrosion performance of steel in concrete. For the U-bend specimens, the HDG performed better than TZD, but it is believed that this is mainly a result of the higher w/c and lower cover which let chloride in too fast preventing the TZD specimen to adequately form a protective passive coating. The HDG coating was thicker and had a chromate treatment which helped it to passivate.

The epoxy-coated TZD bars (TZE) had lower corrosion currents. The damage on the bars was comparable to the TZD in the beam test but did help in the U-bend tests. The coating was not optimized (brushed versus fusion bonded, not formulated for concrete use), which implies that performance could improve with a commercially applied suitable coating.

A summary of the key advantages found for the TZD bars follows:

- Improved corrosion resistance versus HDG at a lower coating thickness (2.6 versus 6.9 mils):
  - Potentially lower initial and life cycle cost due to thinner coating and improved performance.
- Statistically significant lower chloride concentration at the bottom reinforcing bar level for TZD than the other reinforcing bars in the cracked beam tests, indicating that the bars affected cracking below the bar, even though chloride contents were equivalent at the top bars.
- Corrosion potential shift at corrosion initiation similar to that of black bar unlike HDG:
  - Easier to evaluate corrosion condition in the field
  - Better planning for bridge maintenance.
- Corrosion performance of TZD versus HDG reversed in better quality (lower w/c and higher cover) concrete.
- Potential to meet long service life requirements using high performance concrete with TZD or TZE versus using stainless steel bars in conventional concrete for an overall lower life-cycle cost.

The cracked beam tests had several important findings:

- Chloride concentrations decrease with depth if the bar crossing the crack has not exceeded its yield stress, i.e., the bars close the cracks, even when wedged to stay open as the bars are in tension as demonstrated by the crack closing if the wedge is removed. At larger crack sides the bar could yield or lose bond to the concrete and not be in tension. In this case the crack would not close if the wedge was removed.
- Localized corrosion; that is, microcell corrosion on the bars can be significantly greater than the corrosion estimated from just the macrocell current.
- Though the epoxy-coated steel (ECR) performed well, corrosion was initiating on bars without major defects such as intentionally induced damage; for example, drill holes, by the end of the testing.
- Most important is that the test method uses flexural cracks versus pulled smooth wedges which is more typical of cracks in concrete.

Based on the results of this study, the principal investigator (PI) recommends further work with DOTs to initiate trial testing in the field. The cracked beam method looks promising as a test method to evaluate corrosion-resistant reinforcing bars, high-performance concrete, surface treatments and a combination of these. The PI recommends that the flexural cracked beam test be developed into an AASHTO provisional test method specification.

1 IDEA PRODUCT

1.1 INTRODUCTION

Current and future designs for bridges and other reinforced concrete structures exposed to deicing or marine chlorides requires improved corrosion resistance of the reinforcing steels in combination with higher quality concrete. Several stainless steel alloys are believed to have good performance, but the material costs are several times that of conventional black steel. In addition, though only the outer surface of the steel needs protection, the entire bar is made of alloys using premium raw materials.

A more sustainable approach considering initial material costs would be to use black steel with a protective coating, such as in hot-dipped galvanized (HDG) or epoxy-coated bars (ECR). If these bars provide enhanced corrosion protection, there can be a reduction in the overall life cycle cost versus black steel or stainless steel, using holistic approaches addressing the overall performance of the bar as a function of concrete properties and concrete cover over the bars, as performed in life-cycle modeling. These bars are subjected to mechanical damage in placement and in use to due to cyclic loading of the concrete and the development of cracking. The potential for hydrogen embrittlement and coating application temperature limits the use of hot-dipped galvanized coating on some higher strength reinforcing bars that are desired for more efficient designs. Epoxy-coated reinforcement requires longer embedment lengths, and its lower bond might offset the use of higher strength steel bars.

1.2 PRODUCT

The product that was the focus of investigation is a reinforcing bar with a thermal zinc diffusion (TZD) coating, with and without a supplemental organic coating. This TZD coating should have excellent bond to the steel as does the HDG coating, but is applied at lower temperatures than hot-dip galvanizing. This allows TZD coatings to be applied to higher strength steels without negative effects on the strength properties. It has a more porous surface than hot-dipped galvanized so that it should have a better bond to the concrete and is an excellent substrate for paint. The coating is significantly thinner using less zinc.

1.3 POTENTIAL IMPACT ON TRANSPORTATION PRACTICE

TZD-coated reinforcement will have a significantly lower initial cost than stainless steel reinforcement, and can be applied to all strength grades of steel, allowing for potential additional savings where the designer can use higher tensile strengths to reduce the amount of reinforcing bars needed. When used with higher strength bars and lower permeability concrete, TZD could potentially lower the overall upfront and service life costs for bridges versus alternative reinforcing bar options.

2 CONCEPT AND INNOVATION

A process of applying zinc to steel via thermal diffusion has been developed by Distek, NA, and has been in commercial use since 1993. The bars in this study were produced in the United States and coated in Michigan. The coating deposition temperatures (700–780°F) are lower than that in hot-dip galvanizing (840°F), but zinc-iron intermetallic phases form resulting in a metallurgical alloy bond between the zinc overlay and the steel substrate. The process results in a metallurgical conversion of the exterior surface into a porous zinc/iron alloy. The thermal diffusion process provides a very uniform coating that retains the original geometry of the part, as can be seen in Figure 1. It is hard and wear-resistant, and can withstand the rough handling and storage conditions generally expected in the field, as well as exhibiting ductility in bending and forming. Also, the thermal process is not susceptible to hydrogen embrittlement. Tests comparing the performance in severe salt environments with and without abrasion show a 5 to 10 times improvement in performance with the TZD-coated steel versus HDG steel. Steel coated by this method is covered by ASTM A 1059 Standard Specification for Zinc Alloy Thermo-Diffusion Coatings (TDC) on Steel Fasteners, Hardware, and Other Products. Bars can be produced in lengths of 60 ft.

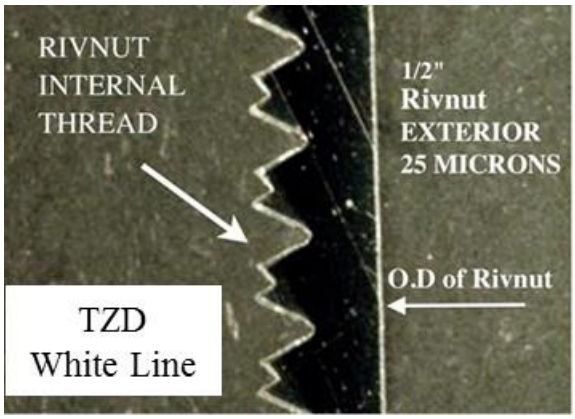

FIGURE 1 Example of how TZD coating maintains the original geometry. Cross section of the nut shows that the internal threads are coated and maintain the thread geometry with a 25-micron coating (bright surface).

Applying TZD to reinforcing bars is a recent application for this technology. The coating is not as thick as the zinc coating in HDG reinforcing bars, which helps to reduce cost and should help in workability. It has excellent abrasion resistance, based on current uses on chains used by the U.S. Navy, and the surface porosity should improve reinforcement bond to the concrete. The higher porosity should be beneficial for a two-component coating where the top coat would be an organic coating.

As noted earlier, the coating is very uniform even over ribs in the bars and is a low-temperature process. This could potentially be applied to higher strength reinforcement. This could potentially result in improved cracking behavior and a reduction in the cross-sectional requirements for the steel. The TZD coating applied to higher strength (grades 75 to 100) reinforcing bars could provide cost savings (less steel required), offsetting the initial upfront cost of the bars, where designs allow for reducing the required reinforcement for higher tensile strength reinforcement.

3 INVESTIGATION

3.1 MATERIAL TESTED

The project review committee suggested replacing the dual coated (zinc plus epoxy) reinforcing bars with ASTM 1035 bars, because dual coated bars were not available. The materials evaluated are shown in Table 1. All of the bars were No. 4, Grade 60 except for the ASTM A1035 bars, which were Grade 100, and the SS bars, which were Grade 75.

TABLE 1 Materials evaluated

Material	Specification(s)	Designation
Thermal zinc diffusion coated steel	ASTM A615	TZD
Epoxy-painted, thermal zinc diffusion coated steel	ASTM A615	TZE
Black Bar	ASTM A615	BB
Epoxy-coated bar	ASTM A706 & A775	ECR
Hot-dipped galvanized bar	ASTM A706 & A767 (Class 1)	HDG
2304 Stainless steel bar (UNS S32304)	ASTM A955	SS
Low-carbon chromium steel bar	ASTM A1035	X35

Unified Numbering System for Metals and Alloys.

The compositions of the reinforcing bars are presented in Appendix A1. The BB and TZD reinforcing bars used the same steel (Nucor, Heat #BR1110214401 June 2011). HDG and ECR bars used the same steel (NUCOR, Heat #KN1310678101, December 2013). The BB bars used alone and as the substrate for TZD met ASTM A 615, the BB used as the substrate for the HDG and ECR bars met ASTM A706. The HDG coating was specified to meet ASTM A767 Class 1 and the ECR to meet ASTM A775. The 2304 SS met the requirements of ASTM A955. The TZE bars were coated manually, with a commercial epoxy (Sherwin Williams Macropoxy 646-100) by the Kentucky Transportation

Center. Photos of the bars are in Appendix 2. There was some rust on the X35 bars as received. Loose rust was removed with wire brushing as can be seen in the photos in Appendix A2.

The TZD, HDG, and ECR coating thicknesses are shown in Table 2. The delta scope (magnetic method) readings did not provide good results for the zinc coatings, due to the rib pattern on the bars, which was close to the probe size. Optical microscopy on ground and polished to 1 micron, cross sections was used to provide a better estimate of the coating and the differences between the two methods were less for the organic coatings. Six to 11 valley and six to 11 web locations were used and averaged. The overall averages combining both locations were used. For coating loss analysis on the TZD and HDG bars, a chemical removal technique was employed as discussed in the experimental and results sections. Figure 2 shows the microstructures of the coated bars.

TABLE 2 Coating thicknesses for TZD, TZE, HDG, and ECR Bars

Bar	**Coating Thickness (mils)**			
	Delta Scope		**Microscopy**	
	Average	**Std. Deviation**	**Average**	**Std. Deviation**
TZD	0.8	0.4	2.6	0.4
TZE	10.4	3.6	9.8	4.0
HDG	2.7	0.6	6.9	3.8
ECR	7.2	1.1	9.3	2.5

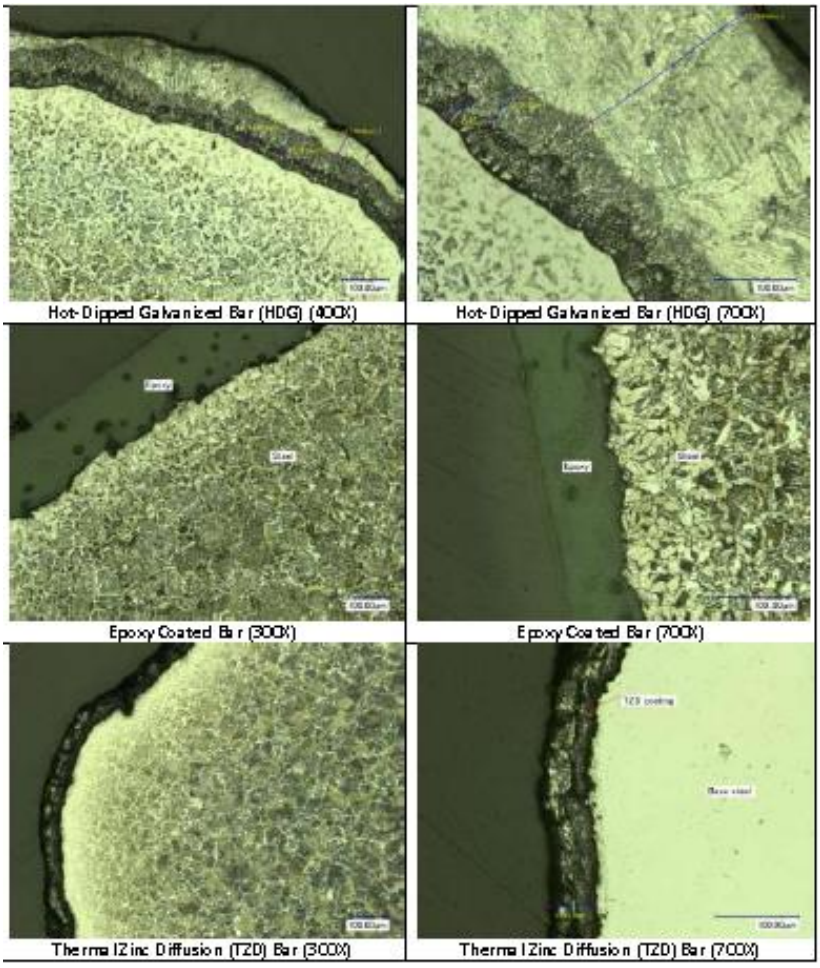

FIGURE 2 Microstructures of the coated bars.

3.2 EXPERIMENTAL PROGRAM

This section describes the properties of the concrete tested, the corrosion specimens, and the corrosion test methods used. Two kinds of specimens were used to evaluate the corrosion performance of TZD and TZE relative to the commercial reinforcing bars in the program. Cracked beam specimens were produced with a good quality concrete mix and reinforcement cover as described below, to simulate cracking that would occur in field concrete. These minibeams were periodically fatigued in flexure, as would be the experience on a bridge deck, even though it is not a part of the deck design in AASHTO LRFD 9.5.3, since fatigue could potentially affect corrosion performance.

Additionally, U-bend specimens were produced at a higher water-to-cement ratio as compared to the minibeams (w/c) and lower concrete cover as compared to the minibeams to obtain results quicker and to evaluate the bars under stress.

The original duration of the test program was to be one year of testing. However, an extension to allow for 2 years of testing was granted because better differentiation of corrosion performance was needed. This can be seen in the following sections.

3.2.1 Concrete Properties

3.2.1.1 Concrete Properties of the Beam Specimens

The concrete mixtures were the same for all the bars evaluated. Specimens were produced for two of the bar types from each batch, except a batch of the TZE bars that were received one month later. Table 3 shows the mixture design for the concrete used to produce the minibeams specimens.

The concrete properties are given in Table 4. There are some minor variations in properties among the four batches used to produce the seven sets of beams. As can be seen in Table 4, the compressive strengths at 28 days were over 5000 psi, and the flexural strengths were over 800 psi, which is representative of a good quality air-entrained concrete mixture. Flexural strengths for the reinforced beams reflect load at cracking. These values are not as accurate as the ASTM C 78 flexural strengths on the unreinforced beams, since the reinforced beams did not break, which made it harder to define the point of the first crack.

TABLE 3 Concrete mixture design for the cracked minibeams

Component	**Units**	**Minibeam Mixture**
Cement I/II	pcy	658
Natural Sand	pcy	1217
Coarse Aggregate 3/4"	pcy	1825
Water	pcy	263
w/c	pcy	0.4
Air	%	6
Slump	inch	4 to 6
Unit Weight	pcf	146.8

The concrete conductivity was determined according to ASTM C 1760, at 14 days when the specimens were tested under flexure and at 28 days. Table 5 shows the conductivities (milli-Siemans/meter, mS/m) as well as the corresponding ASTM C1202 Rapid Chloride values assuming no heating in the C1202 test (C1760 method initial current and with a correction for specimen geometry). The data indicate that the concrete would be in the range of moderate permeability. The projected Coulomb values are higher than might what be typically used as SCMs were not incorporated.

3.2.1.2 Concrete Properties of the U-Bend Specimens

The concrete properties for the U-bend specimens are shown in Table 6. The test schedule for the TZE was delayed one month due to the painting of the bars. The strengths were higher for the second mixture; however, both mixes had similar permeability as seen in the conductivity data shown in Table 5. The conductivity data indicated that the mixes were on the border between moderate and high permeability. This was expected as the w/c ratio was higher for these mixes than that used for the beam specimens.

TABLE 4 Properties of the concrete produced for the cracked minibeams

Mix Description:	**0.4 w/c**			
Batch	**1**	**2**	**3**	**4**
Mix Date:	**3/11/14**	**3/11/14**	**3/12/14**	**4/15/14**
Admixtures				
Grace Daravair M (AEA) oz/cwt	1	1	1	1.2
Grace Daracem 100 (HRWD) oz/cwt	7	7	7	7
Physical Properties				
Slump, in.	6.00	4.75	4.75	4.75
Unit Weight lb/ft^3	145.0	143.8	146.0	144.8
Air, %	6.5	7.3	5.5	5.9
Compressive Strength (C 39)				
1-Day Strength psi (2 each)	2960	2300	2520	2910
14-Day Strength psi (2 each)	5810	5090	5560	5660
28-Day Strength psi (2 each)	6660	5460	6360	5960
Flexural Strength (C 78) Minibeams				
14-Day (psi)	850	725	735	775
28-Day (psi)	925	825	895	830
Cracking Stress of Reinforced C 78 Minibeams **Coated Rebar Specimens**				
TZD 14-Day (psi)	1170			
ECR 14-Day (psi)	1000			
HDG 14-Day (psi)		1150		
TZE 14-Day (psi)				1075
Uncoated Rebar Specimens				
BB 14-Day (psi)		1080		
X35 14-Day (psi)			920	
SS 14-Day (psi)			1080	

TABLE 5 ASTM C1760 conductivity and equivalent
ASTM C1202 permeability for concrete used for minibeams

Conductivity (mS/m)	**Batch Number**			
	1	2	3	4
14 days	18.0	25.8	15.0	16.2
Equivalent Coulombs	3272	4689	2726	2945
28 days	16.6	17.8	14.7	16.1
Equivalent Coulombs	3017	3235	2672	2926

TABLE 6 Properties of the U-bend concrete (mix 6 is for TZE bars)

Mix Description:	**0.5 w/c**	**0.5 w/c**
Batch	**5**	**6**
Mix Date:	**3/18/14**	**4/16/14**
Admixtures		
Grace Daravair M (AEA) oz/cwt	1	0.9
Grace Daracem 100 (HRWD) oz/cwt	5	5
Physical Properties		
Slump, in.	6.00	5.75
Unit Weight lb/ft^3	140.6	143.1
Air, %	6.8	6.5
Compressive Strength		
1-Day Strength psi (2 each)	2010	2110
14-Day Strength psi (2 each)	4600	5290
28-Day Strength psi (2 each)	4840	5960
Conductivity (mS/m)		
1-day	23.0	24.0
Equivalent Coulombs	4180	4362
28-days	22.0	23.0
Equivalent Coulombs	3999	4180

3.2.2 Description of Tests

Two types of corrosion tests were used to evaluate the TZD and TZE bars versus commercial bars in concrete. The test methods and the rationale for using them is discussed below.

3.2.2.1 Cracked Concrete Testing

Several of the accelerated tests conducted in other studies on coated steels intentionally damaged the coatings by drilling holes through the coatings [1–3]. HDG and TZD coatings are very resistant to damage that would go to the black steel, as there is an alloy bond, so such tests might not provide realistic results for actual field applications. In addition, in other experiments, cracks in the concrete were produced using wedges that were pulled out, which does not necessarily represent the morphology of normal cracks [1,2]. The tests in previous studies [1–3] were further accelerated using only 1 in. of cover and typically 0.5 w/c concrete, which may also be unrepresentative of modern field practice.

Studies in Japan and Germany showed that crack size, concrete cover, and concrete quality significantly affect the performance of black steel [4,5]. A study conducted by Berke et al. [6] found similar results in comparing 0.5 w/c cracked concrete with 1 in. of cover to concrete with 1.5 in. of cover. These studies indicate that there is still acceleration of the steel corrosion process using crack sizes at or below the maximum suggested in ACI 224 (0.008 in.) for concrete subjected to deicing salts, in better quality concrete with higher cover. Thus, an accelerated test method that more closely represents actual performance in field applications was used in this study.

To provide accelerated results, the corrosion test method in this study used a concrete cover of 1.5 in. over the bars, at the crack, which is lower than the 2.0 to 3 in. currently being specified in practice. Other means of acceleration include warmer temperatures in the laboratory, versus outdoor temperatures where deicing salts are applied, using the maximum recommended crack size of 0.008 in., and fatigue cycling in flexure to mimic a “working structural crack.”

The concrete for the flexural specimens had a w/c ratio of 0.4 using Type II cement and a 0.75 in. nominal maximum aggregate size. Additional unreinforced minibeams were produced to determine the flexural strength of the concrete and

cylinders for compressive strength. Five reinforced flexural specimens were produced for each type of steel to account for variability in corrosion testing.

The flexural specimens consisted of 20 × 6 × 6 in. concrete minibeams that have one bar on the top mat and two bars to provide the cathode on the bottom mat. All bars were #4 deformed bars (0.5 in. in diameter) and were to be preconditioned by rotation in a container of coarse aggregates, to simulate abrasion of the concrete aggregates during field placement. A 1/8 in. deep notch was cut across the top in the center and the minibeams were third-point loaded to generate a crack that was 0.008 to 0.01 in. wide. Minibeams were loaded and unloaded 5 times to 75 percent of the flexural strength. After flexing, shims were inserted to keep the crack open and to apply a small stress to the bars. The sides were sealed with epoxy and a dam (reservoir) was applied to the surface. Concrete cover over the bar at the bottom of the notch was 1.5 in. Figure 3 is a schematic of the specimens.

The initial crack openings for the minibeams are in Table 7. The cracks did not go beyond the yield strength of the bars (presumed to be the case as the cracks closed when the load was removed) so the bars were exerting a force to close the cracks. Plastic shims were used to keep the cracks from closing. The cracks were in the range of 0.005 to 0.015 in. It is difficult to control crack opening so the range is slightly larger than the desired range of 0.008 to 0.01 in., with one SS and one HDG specimen having high values compared to other specimens, but still with low values for others.

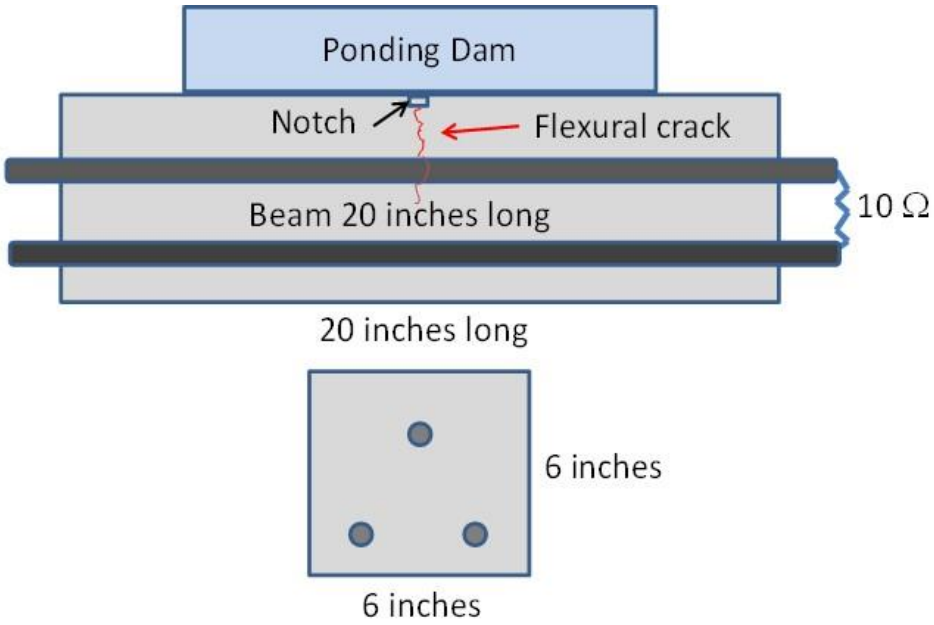

FIGURE 3 Side view schematic of crack specimens with a dam on top and crack.

TABLE 7 Surface crack widths for the cracked minibeams specimens

Beams	**Average Crack Width (mils) for Group of Beams**		**Extreme Crack Widths (mils) for Group of Beams**	
	Avg.	Std. Dev.	High	Low
BB	0.009	0.002	0.010	0.005
SS	0.013	0.005	0.020	0.007
X35	0.007	0.002	0.010	0.005
ECR	0.010	0.002	0.015	0.007
HDG	0.013	0.006	0.025	0.005
TZD	0.008	0.002	0.010	0.005
TZE	0.010	0.002	0.012	0.008

The specimens were ponded for one week with 3% NaCl and then dried for one week, and the cycle was repeated. The current between the top and bottom bars measured by the voltage drop across a 10-ohm resistor, also called macro-cell current, was to be measured at the end of the wet week as modified from the original proposal by the review committee. The corrosion potential was measured using a copper/copper sulfate (Cu-$CuSO_4$, or CSE) reference electrode (ASTM C876). After the wet portion of every six cycles, the dams were removed, and the specimens were flexed five times to 75 percent using 4-point loading of the 28-day flexural strength for the specific concrete mixture for each beam. Dams were reapplied and the testing continued with cyclic ponding.

Two specimens of five were removed for an autopsy at 34 cycles (68 weeks). The TZE specimens were removed at 36 weeks. The rest of the specimens remained in testing for 52 cycles (2 years) of testing. The autopsies included chloride analysis at and away from the cracks, a corrosion evaluation of the bars (amount of rust and degree of rust), and microscopy of the coated specimens.

3.2.2.2 Evaluation of Bent Bars Under Stress

Bars were bent in a U-bend as in ASTM G 30 Standard Practice for Making and Using U-Bend Stress-Corrosion Test Specimens. Figure 4 shows a schematic of the specimens that consisted of a bar with a U-bend, placed in a rectangular concrete block. The concrete cover over the reinforcement was only 1.0 in. to accelerate the ingress of chloride and a concrete with a w/c = 0.5 was used to further accelerate testing because of relatively higher porosity. A higher w/c concrete is being used here to decrease the time for chloride ingress, since these specimens were uncracked. The bend was a 5-d diameter, without over-bending, so the ends were pulled in keeping the bars under stress. After bending the bars, micrographs, and photos of the bent area were taken to document the condition before corrosion testing.

The HDG coatings on reinforcing bars could crack in bending so mandrel diameters are typically 6-d or larger according to ASTM A767. ASTM A615 allows mandrel diameters to 3.5-d for bars up to Grade 60 and 5-d for bars up to Grade 80. The larger mandrel diameters for bending galvanized bars are to lessen the cracking damage caused by bending of the coating, which could adversely affect corrosion resistance. ECR can use the same bending diameters as HDG bar, but some crazing of the coating might occur.

The bars were not bent beyond 180 degrees and released to reduce stress, so the holder on the top of the specimens in Figure 6 was used to keep the bars vertical in the specimens. The X35 bar had a stress in excess of 90,000 psi because it does not have a typical yield point and it was not over-bent and released. This is far beyond what would be used in the field and was not realized to be the case at the time.

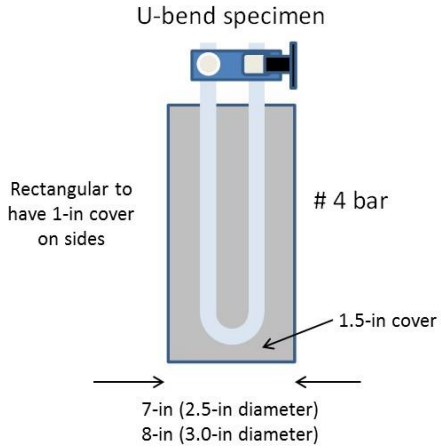

FIGURE 4 Schematic of 9-in. tall (concrete portion) U-bend specimens. Specimens were 7-in. wide for 2.5 in. diameter bends, and 8-in. wide for 3.0-in. diameter bends.

The appearance of the coated bars after bending is shown in Figure 5. The TZE coating did not have good adhesion at the bends as it was applied manually and was not optimized for this application. The TZD, HDG and ECR coatings looked good.

The U-bend specimens were partially ponded in 4.5-in. of 3% by weight NaCl solution in water (half the concrete specimen height). Corrosion potentials were measured on a monthly basis. Polarization resistance and electrochemical impedance spectroscopy (EIS) were performed initially after 1 month, and then at three month intervals or when corrosion was indicated in the corrosion potential tests. Specimens were removed for an autopsy at 17 months (two of five specimens) and at two years.

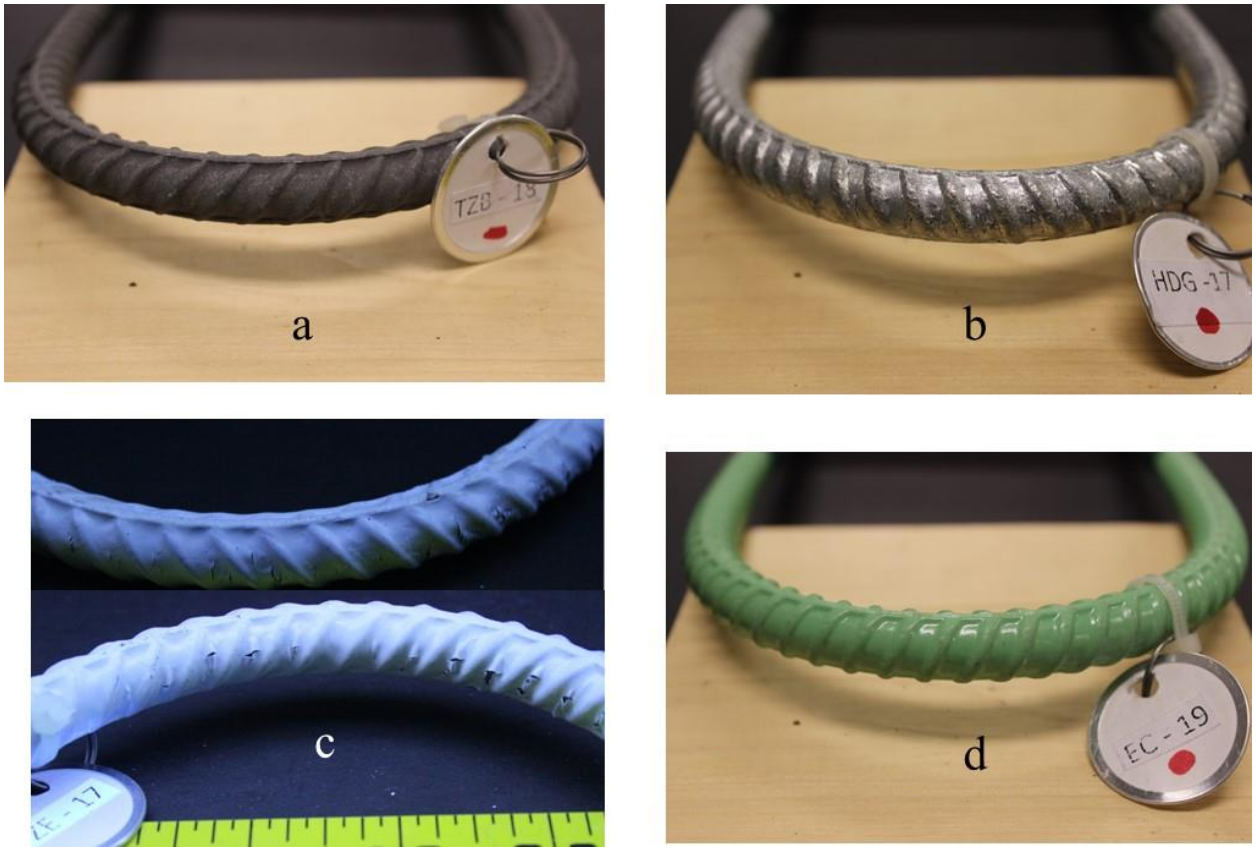

FIGURE 5 Coated bars after bending: (a) TZD; (b) HDG; (c) TZE; (d) ECR. Only TZE bar showed severe cracks and defects in both the tension and compression sides of the bend.

3.3 RESULTS AND DISCUSSIONS

3.3.1 Cracked Minibeams

3.3.1.1 Electrochemical Corrosion Tests

Corrosion potentials, macrocell corrosion currents between the top and bottom bars, chloride distributions, a percentage of rust and mass loss tests were conducted. The tests ended after 52 cycles (two weeks/cycle). Two of the five specimens were removed before the end of the testing for a preliminary analysis at 34 cycles (36 for TZE). A picture of the minibeams is shown in Figure 8.

Table 8 provides the average corrosion potential data for the minibeams over time, and Tables 9 and 10 provide the average macrocell currents. The difference between Table 9 and Table 10 is that some specimens had reverse macrocells (top bar acting as a cathode to the bottom bar), so Table 10 shows the absolute value of the measured macrocell current.

FIGURE 6 Cracked beam corrosion specimens. Specimens are 6 in. x 6 in x 20 in.

TABLE 8 Average corrosion potentials versus time for the cracked minibeams

Up-to-Date Macrocell Data for TCG 13132 (NCHRP-IDEA)							
	BB	EC	X35	SS	HDG	TZD	TZE
Cycle No.	Halfcell Potential (mV vs CSE)						
	(mV)	(mV)	(mV)	(mV)	(mV)	(mV)	(mV)
1	-415	-305	-204	-201	-896	-460	-449
2	-431	-294	-213	-203	-853	-367	-432
4	-403	-184	-201	-195	-758	-303	-344
6	-390	-176	-192	-191	-691	-291	-318
8	-395	-125	-279	-190	-670	-280	-318
10	-393	-133	-279	-189	-627	-255	-272
12	-375	-80	-279	-172	-569	-232	-274
14	-377	-77	-271	-178	-561	-228	-295
16	-383	-75	-284	-177	-534	-213	-298
18	-372	-63	-269	-171	-498	-209	-331
20	-382	-66	-289	-175	-518	-209	-322
22	-383	-66	-271	-182	-491	-212	-313
24	-379	-55	-275	-176	-482	-197	-334
26	-393	-263	-305	-178	-490	-208	-359
28	-385	-280	-311	-178	-474	-200	-337
30	-381	-292	-297	-186	-473	-209	-352
32	-385	-294	-318	-187	-474	-246	-344
34	-373	-257	-302	-191	-471	-272	-315
36	-353	-389	-311	-182	-411	-256	-333
38	-357	-407	-315	-170	-430	-249	-330
40	-346	-389	-292	-165	-389	-243	-324
42	-314	-362	-254	-158	-371	-225	-321
44	-356	-408	-279	-160	-389	-238	-330
46	-339	-392	-256	-148	-362	-224	-319
48	-330	-374	-248	-145	-354	-221	-341
50	-363	-392	-257	-156	-380	-230	-332
52	-349	-408	-262	-158	-378	-231	-317

For uncoated steel reinforcement, corrosion potentials more negative than −350 mV vs. CSE are typically related to the breakdown of passivity. According to ASTM C876, corrosion potentials lower than −350 mV CSE indicate a 90 percent probability of corrosion occurring at the time of measurement. All of the BB specimens clearly went into corrosion on the first cycle and this is reflected in the average corrosion potentials in Table 8 and the macrocell currents in Tables 9 and 10. Note that based upon the exposed area of the top bar, a macrocell current of 10 µA is equivalent to 0.1 µA/cm^2, and the initiation of corrosion. The comparison of the average corrosion potentials to the average macrocell current is not as straightforward for the other specimens.

TABLE 9 Average macrocell data versus time for the cracked minibeams

Cycle No.	BB		EC		X35		SS		HDG		TZD		TZE	
	Macrocell Current and *Integrated* Macrocell Current On Top Bar													
	(µA)	*(Coulombs)*	(µA)	*(Coulombs)*	(µA)	*(Coulombs)*	(µA)	*(Coulombs)*	(µA)	*(Coulombs)*	(µA)	*(Coulombs)*	(µA)	*(Coulombs)*
0		0		0		0		0		0		0		0
1	-115	35	1.0	0	-12	4	0.0	0	38	5	-191	58	0	0
2	-138	188	0.0	0	-10	16	0.0	0	-34	55	-82	223	7	4
4	-138	522	-1.0	1	-9	8	0.0	0	-45	196	-56	391	2	15
6	-105	815	0.0	2	-7	59	1.0	0	-12	283	-32	497	2	20
8	-112	1077	0.0	2	-51	130	1.0	0	-24	336	-32	575	5	28
10	-97	1330	0.0	2	-57	261	-2.0	3	-12	382	-17	633	2	35
12	-77	1541	0.0	2	-45	384	0.0	6	3	404	-7	662	1	38
14	-67	1715	0.0	3	-38	484	0.0	6	3	413	-7	678	0	39
16	-47	1853	-1.0	4	-43	582	1.0	6	-1	423	-6	693	1	41
18	-44	1967	-2.0	7	-39	682	0.0	6	1	433	-4	706	2	44
20	-34	2065	1.0	9	-46	786	-0.9	8	0	440	-4	719	3	50
22	-23	2139	-0.7	9	-42	892	-11.2	22	-2	449	-4	725	-2	56
24	-17	2198	1.2	10	-38	989	1.4	36	-4	459	-2	731	-3	63
26	-25	2259	0.2	10	-42	1086	-0.2	36	1	467	-2	736	-2	69
28	-20	2322	-1.6	12	-43	1190	-0.2	37	-1	471	-4	744	-3	75
30	-33	2389	-0.9	15	-44	1296	0.1	37	0	475	-4	754	-5	84
32	-41	2478	0.4	16	-51	1411	2.8	37	0	478	-29	793	-3	93
34	-37	2574	0.3	17	-46	1529	-0.4	38	-1	482	-74	918	-5	103
36	-31	2097	0.5	17	-56	1535	0.3	39	2	390	-53	928	-8	118
38	-30	2171	-0.2	17	-52	1666	-0.3	39	-2	395	-59	1063	-3	119
40	-38	2253	-0.4	18	-35	1771	-1.1	41	0	399	-51	1197	-1	124
42	-28	2332	-1.1	19	-22	1841	-0.1	42	-1	402	-46	1315	-2	128
44	-41	2415	-0.6	22	-29	1903	-0.3	43	-1	405	-52	1434	2	131
46	-39	2512	-0.8	23	-26.3	1970	-1.3	45	-1	407	-48	1555	3	137
48	-31	2596	-0.5	25	-26.6	2034	-0.1	47	-1	411	-48	1670	1	142
50	-23	2661	-0.4	26	-26	2098	-0.4	47	-5	419	-46	1784	3	147
52	-22	2733	-0.2	27	-29	2164	0.1	48	-5	435	-45	1935	3	155

Figure 9 shows a plot of the average integrated macrocell currents including the currents on all the bars. All of the corrosion-resistant reinforcing bars outperformed BB. The slope of the curves is the macrocell corrosion rate and it shows a decrease for the BB after 200 days. This can be attributed to re-passivation of the BB, corrosion products reducing the rate of corrosion, or to corrosion of the bottom bars that would reduce the cathode area available for macrocell corrosion. As will be shown later, the corrosion of the bottom bars is the most likely cause for this behavior.

The HDG and TZD showed high initial corrosion rates as indicated in Tables 9 and 10 and Figure 7. This is due to the zinc coating developing a protective oxide. The TZD is a more porous coating, so the current would be higher than for the HDG as more surface area is present. Since a macrocell was present it indicates that the zinc coatings passivate quicker in the absence of chloride. Once the oxide was formed the corrosion rates became equivalent to that of SS until the severe corrosion reinitiated due to higher chloride values. There was a period of low corrosion until the zinc coatings were penetrated. The TZD coating was less than half the thickness of the HDG coating so it would be expected to behave as shown.

The ECR, SS, HDG and TZE bars showed the least macrocell current. This would be expected for ECR and TZE as coated steel will do well in a short time test of this nature. However, as will be shown in later sections, corrosion did

occur on both TZE and ECR. The increase in total corrosion current was 48% for ECR, 41.7% for SS, and 73.1% for HDG, comparing values in Table 10 with Table 9.

TABLE 10 Average macrocell data versus time for the cracked minibeams including macrocell current on the bottom bars

Cycle	BB		EC		X35		SS		HDG		TZD		TZE	
No.	(µA)	*(Coulombs)*	(µA)	*(Coulombs)*	(µA)	*(Coulombs)*	(µA)	*(Coulombs)*	(µA)	*(Coulombs)*	(µA)	*(Coulombs)*	(µA)	*(Coulombs)*
0		0		0		0		0		0		0	0	0
1	115	35	1.0	0	12	4	0.0	0	73	22	191	58	0	0
2	138	188	0.0	1	10	16	0.0	0	95	124	82	223	7	4
4	138	522	1.0	2	9	39	0.0	1	60	311	56	391	2	15
6	105	815	0.0	3	7	59	1.0	2	27	416	32	497	2	20
8	112	1077	0.0	3	51	130	1.0	4	26	479	32	575	5	28
10	97	1330	0.0	4	57	261	2.0	7	16	529	17	633	2	35
12	77	1541	0.0	5	45	384	0.0	10	10	561	7	662	1	38
14	67	1715	0.0	6	38	484	0.0	11	11	586	7	678	0	39
16	49	1854	1.0	7	43	583	1.0	13	9	610	6	693	1	41
18	48	1971	2.0	10	39	682	0.0	14	8	630	4	706	2	44
20	37	2073	0.8	13	46	786	0.9	16	6	646	4	716	3	50
22	28	2151	0.7	14	42	893	11.2	30	6	660	4	725	2	56
24	30	2220	1.2	17	38	989	1.4	45	6	675	2	731	3	63
26	31	2293	0.2	18	45	1087	0.2	47	4	687	2	736	2	69
28	26.5	2363	1.6	21	43	1190	0.5	48	3	695	4.2	744	3	75
30	32.5	2434	0.9	24	44	1296	0.3	49	3	702	4	754	5	84
32	41	2523	0.6	25	51	1411	2.8	53	3	709	29	793	3	93
34	39.9	2621	0.6	27	46	1529	0.5	57	3	716	73.8	918	5	103
36	31.3	2178	0.5	29	56	1535	0.3	59	5	698	52.9	928	8	118
38	29.9	2252	0.3	30	52	1666	0.3	60	4	708	59	1063	3	119
40	37.6	2334	0.4	31	35	1771	1.1	61	2	714	51.4	1197	1	124
42	27.8	2413	1.1	32	22	1841	0.1	63	2	718	46.4	1315	2	128
44	41.9	2497	0.6	35	29	1903	0.3	63	1	721	52.2	1434	2	133
46	38.8	2595	0.8	36	26	1970	1.3	65	1	724	47.6	1555	3	139
48	30.6	2679	0.5	38	27	2034	0.1	67	2	728	47.83	1670	1	144
50	22.7	2743	0.4	39	26	2098	0.4	68	5	736	46.37	1784	3	149
52	21.5	2816	0.3	40	29	2164	0.1	68	5	753	45.27	1935	3	157

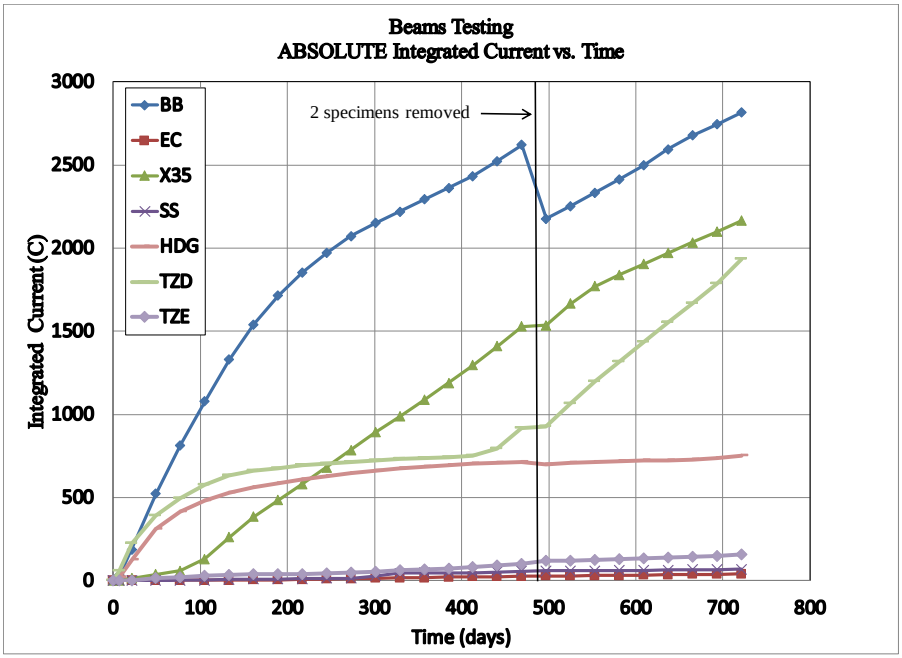

FIGURE 7 Total integrated macrocell current over time.

The variation in the data is shown in Figures 8–15, which give the corrosion potentials, macrocell currents, and integrated macrocell currents for each series of bars. As noted**,** two minibeams of each bar type were removed for autopsy at 34 cycles; therefore, three minibeams were tested for the entire 52 cycles (2 years).

A rule of thumb is that cracking due to corrosion could occur at approximately 1 mil (0.001 in.) of bar loss, which corresponds to 68.4 Coulombs/cm^2 or 6900 Coulombs [11,12]. The macrocell corrosion only reached half that value for some of the black bar specimens. The corrosion potential data has little scatter but there is more scatter in the current data, which can vary by over an order of magnitude in corrosion testing, which is one reason for testing five specimens.

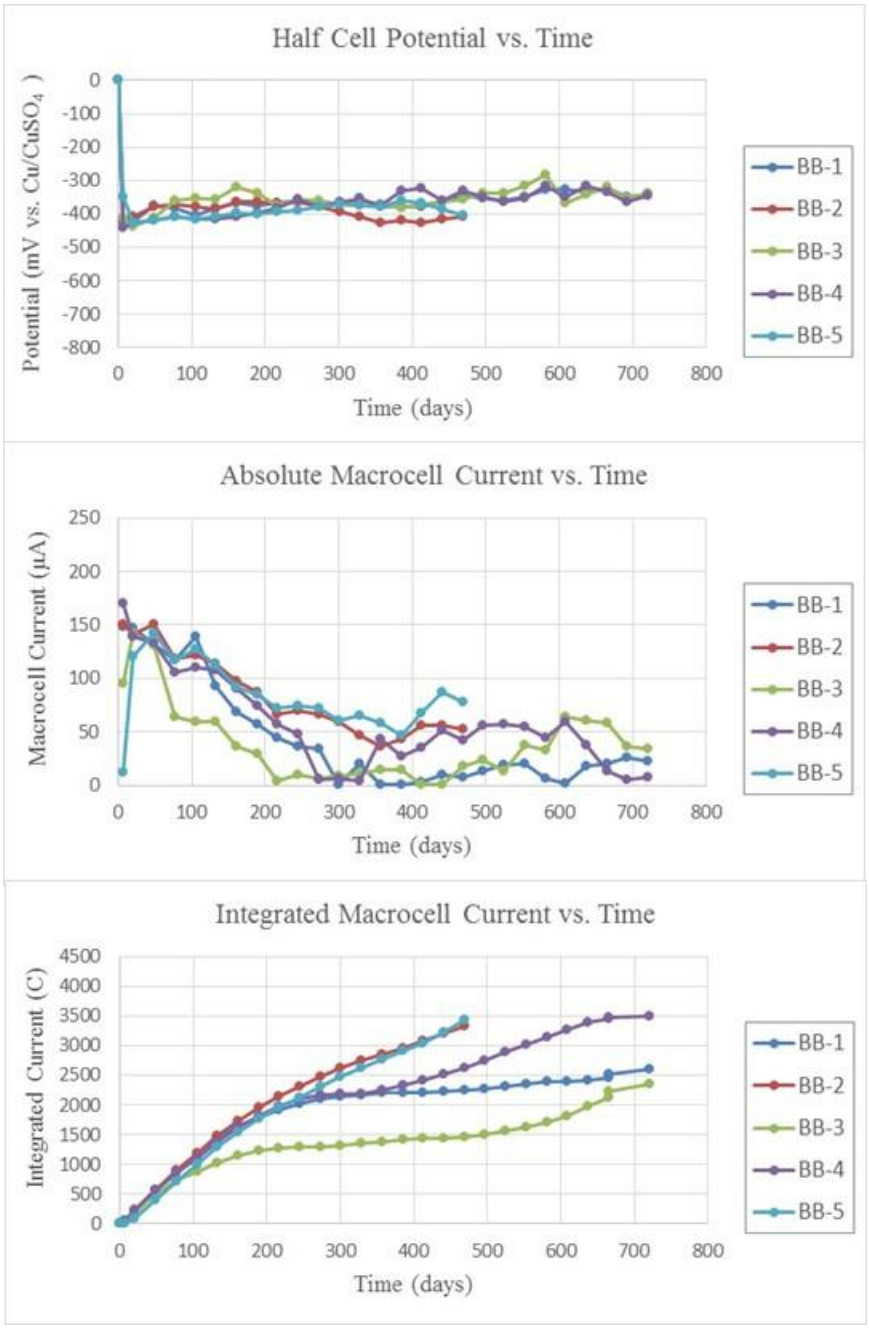

FIGURE 8 Macrocell data for BB cracked minibeams.

Figure 9 provides the macrocell data for the TZD cracked minibeams. Only two of the five minibeams had severe macrocell corrosion, which initiated at a later point than seen for all the BB specimens corroding. As noted earlier, scatter in corrosion data are expected once specimens start to corrode. The initial corrosion potentials start negative as the zinc is

passivating. When the current decreased to passive levels the corrosion potentials were in the range of passive steel in concrete. This might be due to the nature of the coating, which is a zinc-iron intermetallic and not pure zinc. When corrosion did initiate there was a sharp decrease in potential to those associated with corrosion of black bar and as seen on the BB specimens. This is a good means to monitor performance, which as will be shown is not the case for HDG.

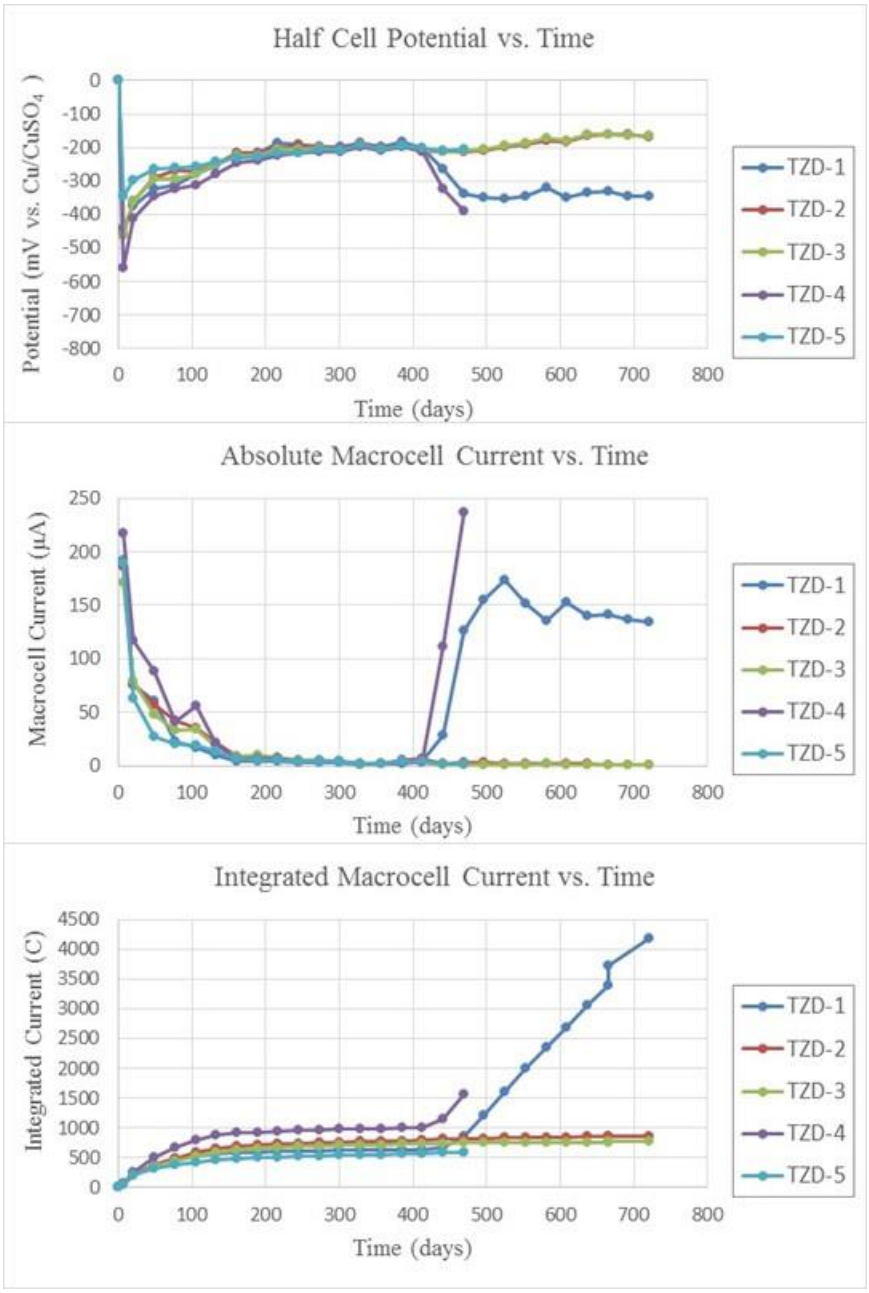

FIGURE 9 Macrocell data for TZD cracked minibeams.

The macrocell corrosion rates for the three TZD passive bars were very similar to those of SS bars as will be shown later. Though the corrosion rate for corroding bars appeared to be higher than that for some BB bars, this is due to the bottom bars providing more of the cathode as their corrosion rate is low.

Figure 10 shows the corrosion behavior for the HDG minibeams. Scatter in corrosion data is not unexpected, and could be due to differences in chloride contents in the individual specimens, and local variations in the concrete. Even the two corroding TZD specimens outperformed the best control specimens.

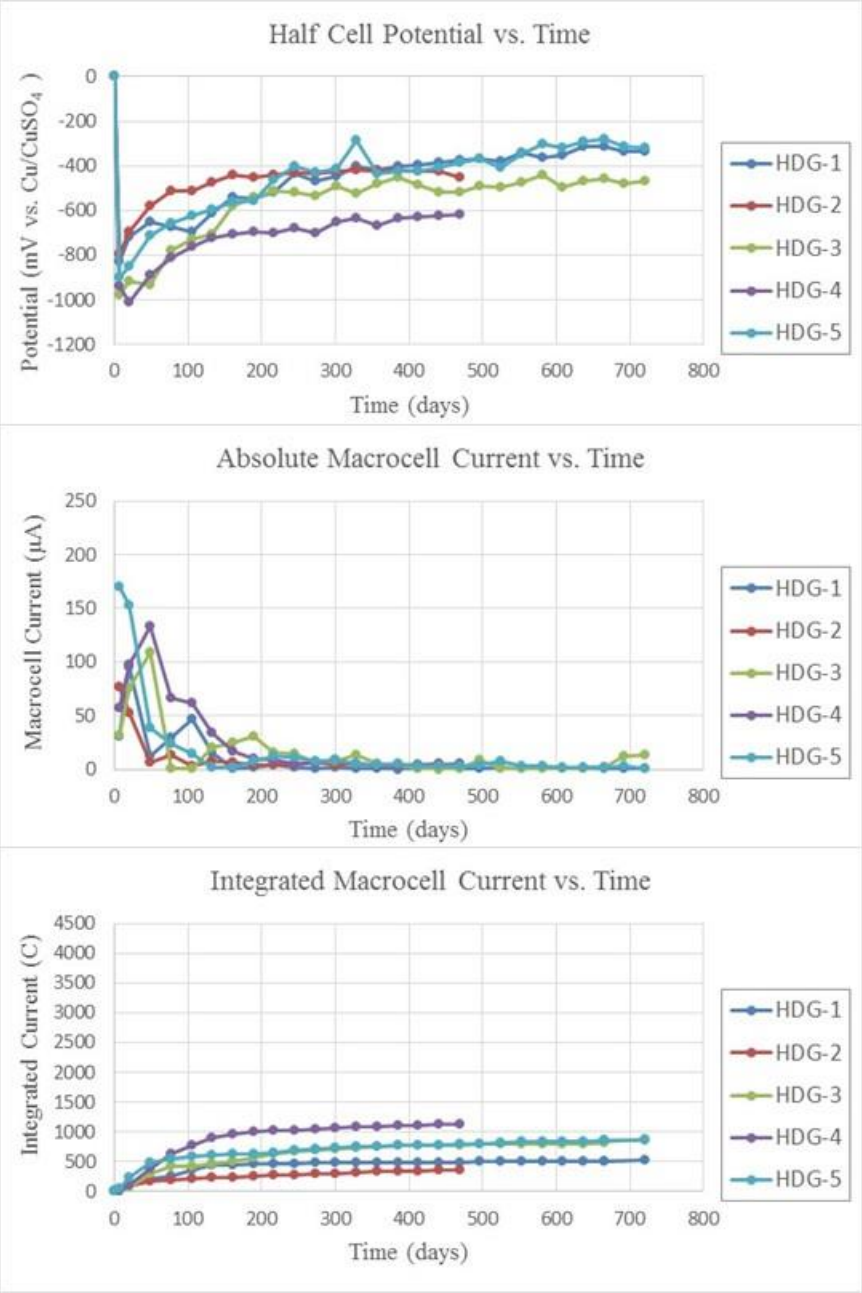

FIGURE 10 Macrocell data for HDG cracked minibeams.

The corrosion performance of HDG initially was similar to TZD, which indicated high currents and low negative potentials. However, the zinc coating passivated potentials did not become more positive than −350 mV vs. CSE, so there is not a set potential above which passivation is indicated, as was the case for TZD. The macrocell current behavior indicates better performance than the TZD. Some of this would be due to a higher coating thickness, and as will be shown later and can be seen in comparing total Coulombs in Table 9 with Table 10, there was considerable macrocell corrosion rates on the bottom bars indicating that the macrocell currents are not indicative of all of the corrosion.

The addition of a non-optimal hand-painted, epoxy coating to the TZD considerably reduced macrocell current as seen in Tables 9 and 10 and Figure 7. Figure 11 provides the macrocell data for the individual specimens. The current axis and integrated current axis are on a different scale than that used for the BB, TZD, and HDG specimens, in Figure 11, to reflect the much lower currents for TZE.

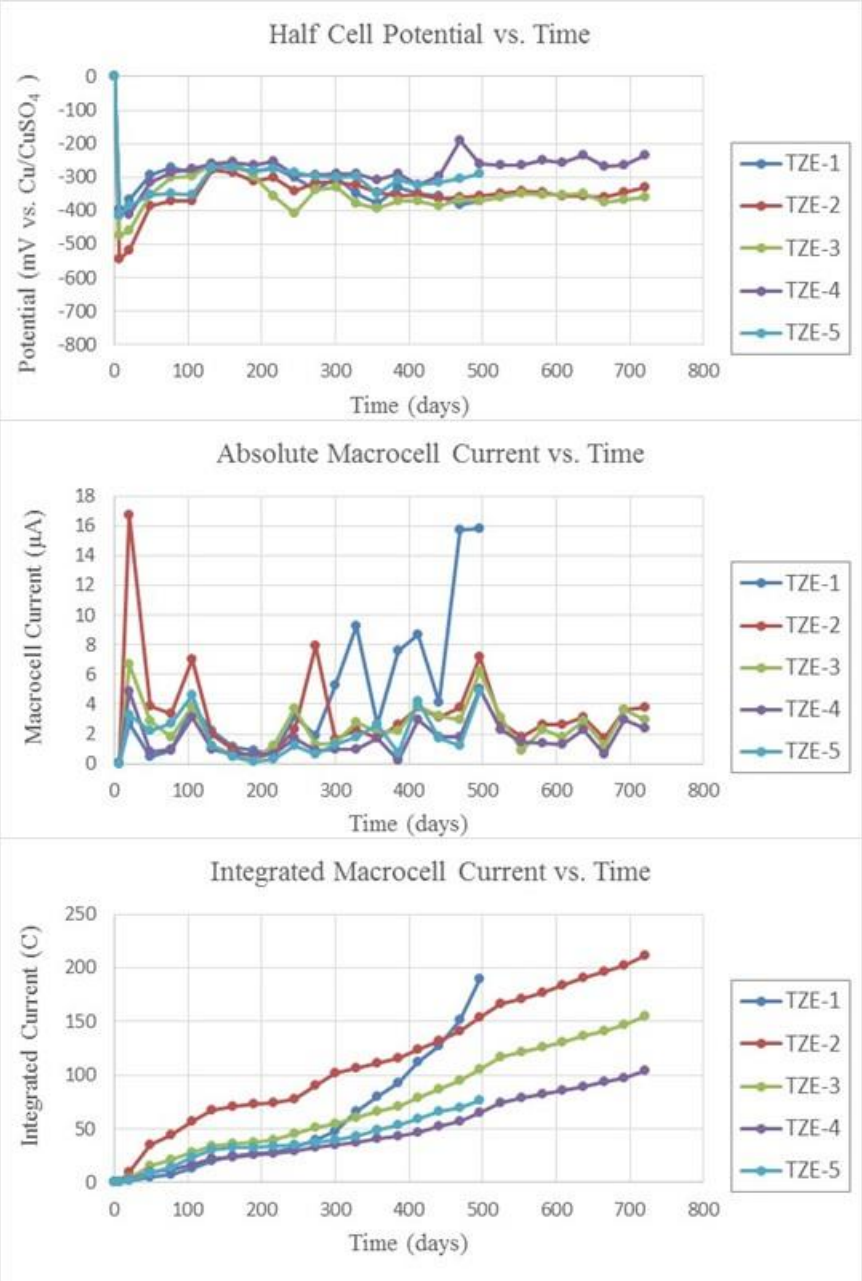

FIGURE 11 Macrocell data for TZE cracked minibeams.

It is difficult to find a relationship between corrosion potential and the macrocell corrosion for the TZE bars, most likely due to the organic coating present. The specimen with the lowest current (TZE 4) did, however, have a corrosion potential more positive than −300 mV CSE. The overall macrocell currents are very low indicating that it would take several years of accelerated corrosion testing to cause damage to the concrete if the corrosion rate remained in this range. As in any product with a nonconductive barrier coating, such as the ECR specimens in this study, the corrosion currents are primarily concentrated at the flaws, so corrosion rates are higher at those locations.

The ECR individual specimen macrocell data are in Figure 12. The test method is not as severe to these bars as the other bars, as coating failure mechanisms are often due to aging effects of the coating, which takes several years to occur. Also, as the ECR bars have specification requirements for the coating system, including limits on allowable defects, they were less damaged by the pretreatment techniques than the TZE bars. As such the currents and integrated currents for the ECR bars as shown in Figure 12 are very low, even lower than what was observed for the SS bars as can be seen in Tables 9 and 10.

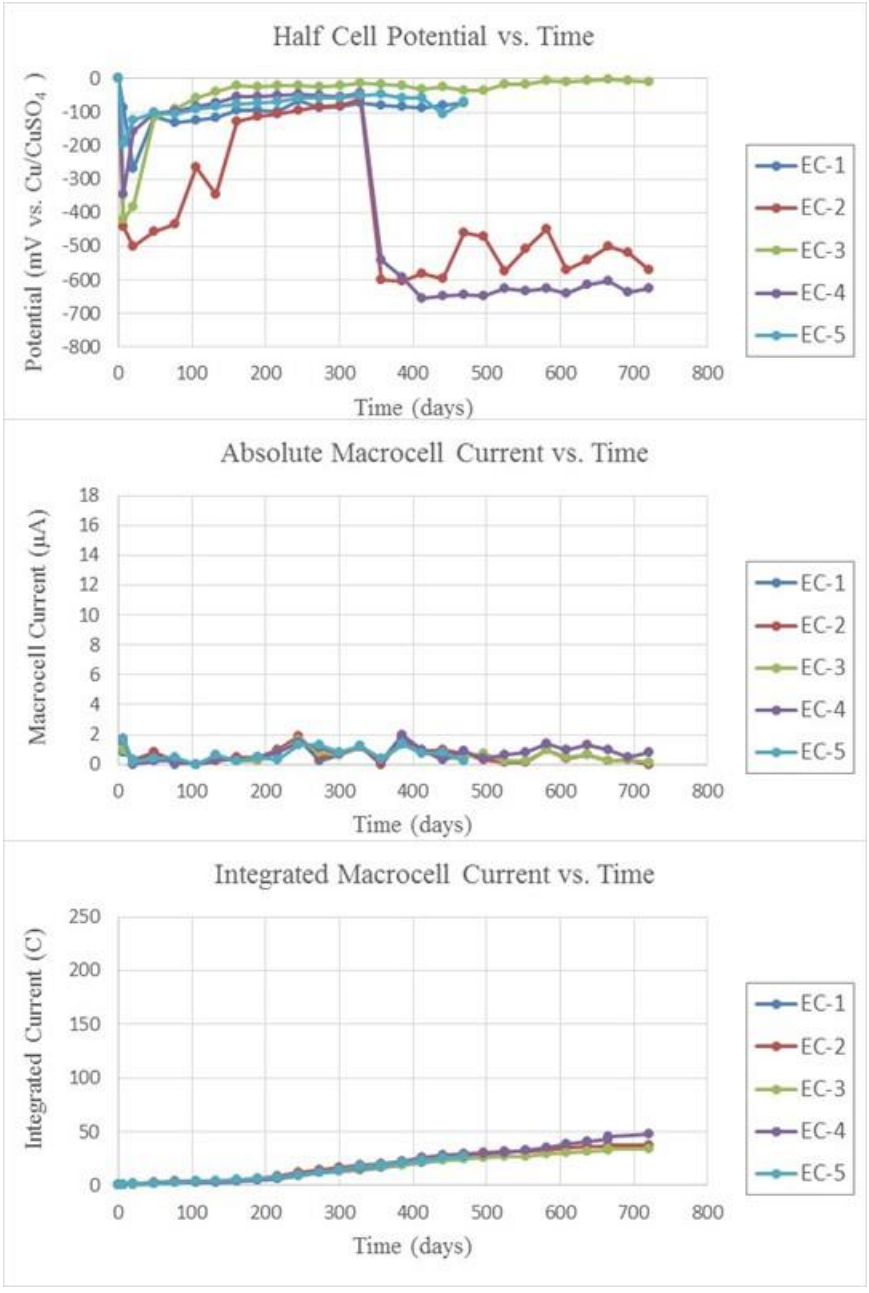

FIGURE 12 Macrocell data for ECR cracked minibeams.

The ECR minibeams as noted had very low macrocell corrosion, but it was not zero, indicating that some current is generated at locations of coating through defects. The corrosion potential data showed initially high negative potentials that then came into the range where BB is considered to be passive. This indicates that oxygen and liquid are passing through the coating, but not chloride. A large decrease of potential for two of the specimens occurred after about a year of testing. This indicates that some corrosion might be occurring, but not being identified in the macrocell data. This will be addressed when the autopsy results are discussed.

The other two commercial alloys tested were the X35 and SS bars. Figure 13 provides the macrocell data for the X35 specimens. Corrosion initiation occurred between 105 and 357 days, which was a considerable improvement over the BB specimens. Comparing the corrosion potentials to when the macrocell current was approximately 10 µA or lower indicates that the potential below which the bars are active in this set of experiments is approximately −280 mV vs. CSE. The higher value than for BB might be due to the chromium content in the passive oxide that forms on the X35 bars.

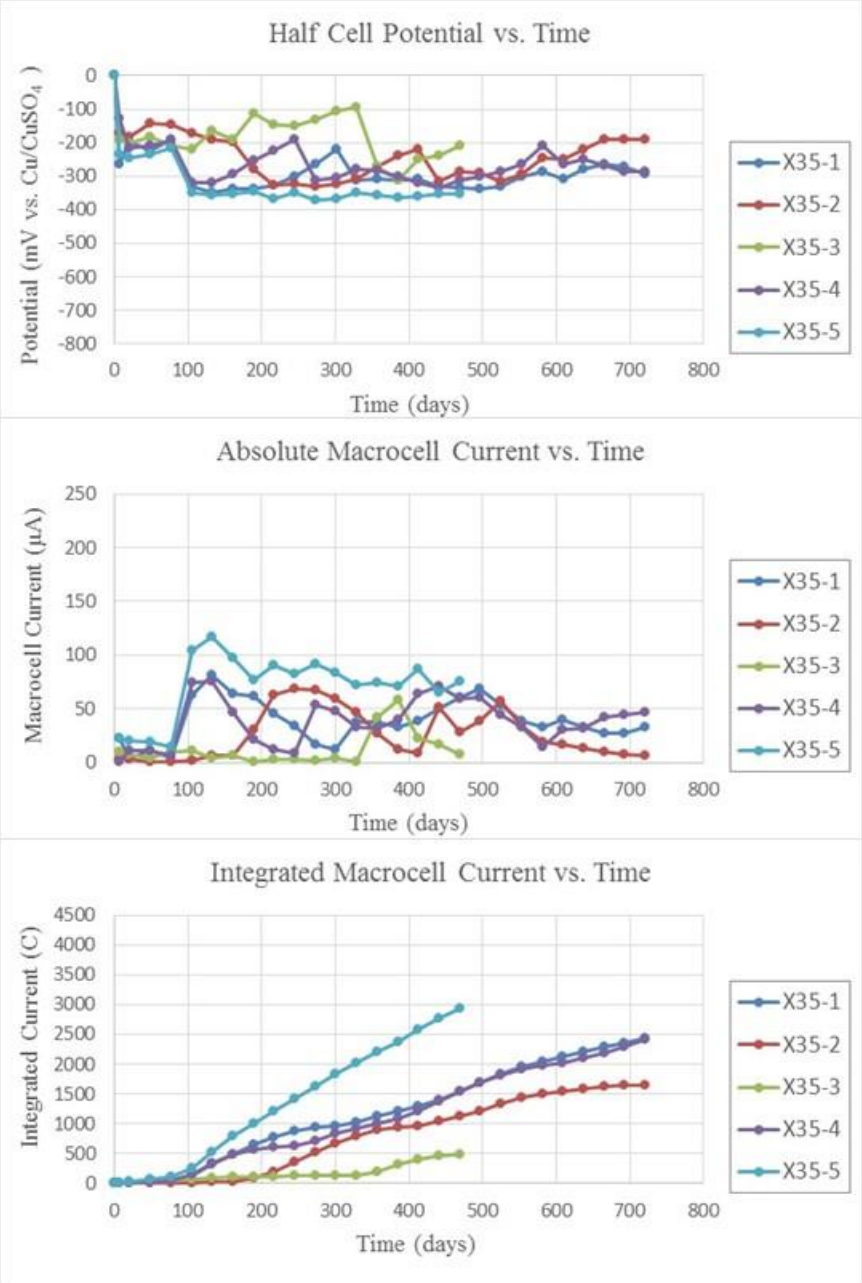

FIGURE 13 Macrocell data for X35 cracked minibeams.

The results for the X35-2 specimen as shown in Figure 13 indicate that the bar re-passivated as the current decreased and the corrosion potential moved to the passive region. Since there were no reverse macrocells, this indicates that the bar is passivating, perhaps due to surface enrichment in chromium as the iron corrodes. Similar behavior was found for X35-3 before it was removed.

The SS specimen macrocell data are shown in Figure 14. The macrocell corrosion rates were low and the half-cell potentials were in the passive region for all the specimens. However, there were a few times when the currents jumped indicating that some corrosion might have initiated then re-passivated. Only at 301 days did the currents exceed 10 µA.

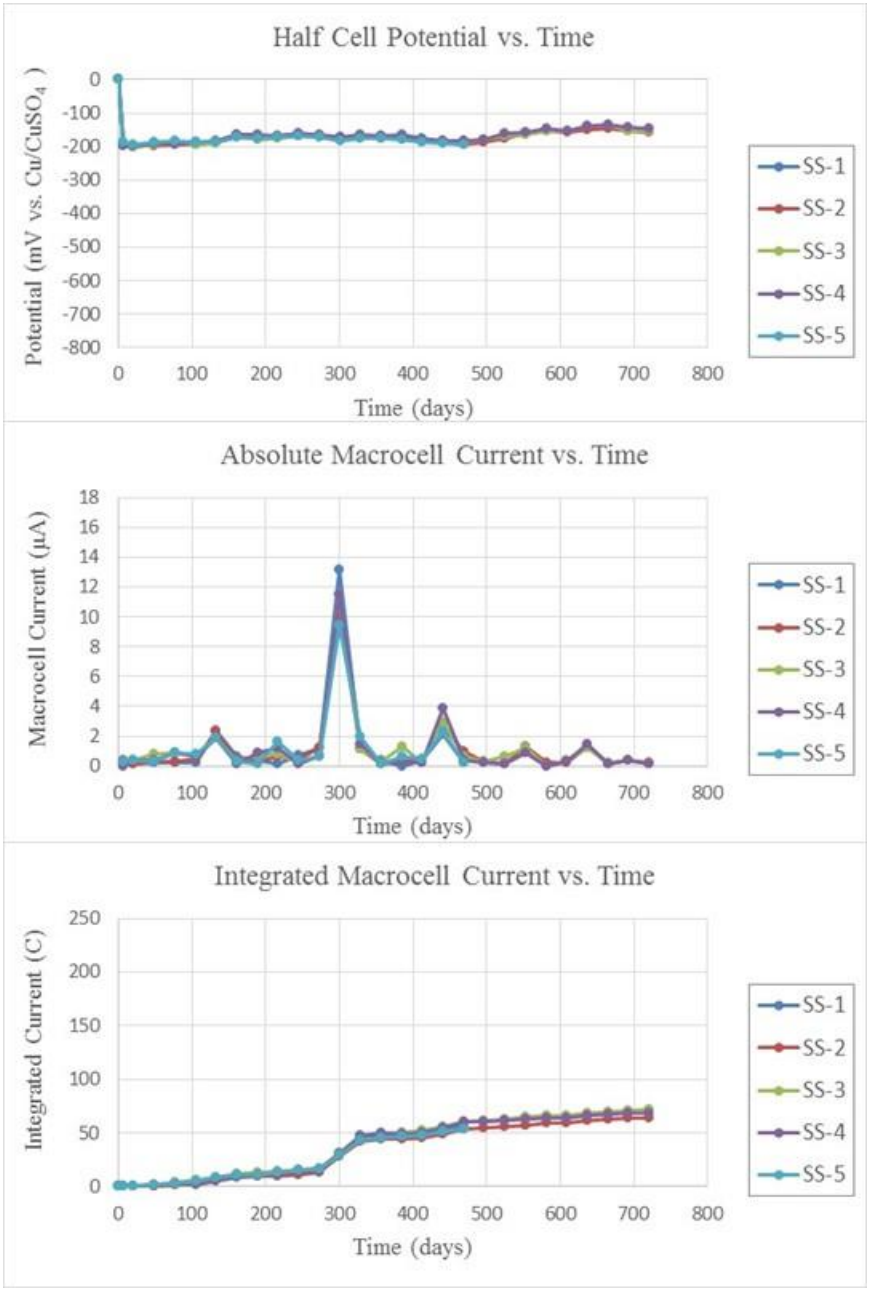

FIGURE 14 Macrocell data for SS cracked minibeams.

3.3.1.2 Appearance and Autopsy Results

3.3.1.2.1 Cracks

In the process of testing, some cracking occurred on some of the cracked minibeams. Table 11 shows a synopsis of the cracking data. These cracks formed within the first year of testing and did not change after that. Figure 15 shows one of the most severe cracks that formed on an HDG specimen.

TABLE 11 Crack summary on minibeams after one year of testing including fatigue for five minibeams total of each bar type.

	BB	ECR	X35	SS	HDG	TZD	TZE
No. Cracked	3	2	1	1*	4	2	0
No. ≥0.004 in.	0	1	0	0	2	0	0
Length (in.)							
Crack 1	2	4	CI		3	CI	
Crack 2	CI	4			2 (CI)	< 2*	
Crack 3	2				2		
Crack 4					2 (CI)		

CI =Chipped at insert

*Crack is perpendicular to bar

FIGURE 15 Crack on one of four HDG minibeams that cracked in testing.

The best performing bars are the X35, TZD, SS, and TZE. As shown in Table 11 cracking was more severe on the HDG and BB. The longest crack lengths were for ECR. None of the specimens had rust staining or cracking at the surface. Given the earlier discussion about the amount of integrated current, this is as would be expected.

3.3.1.2.2 Autopsy results

Two minibeams of five were removed after 34 cycles (36 cycles for TZE), for an autopsy. Table 12 shows the acid soluble chloride content, based on mass of the concrete, at the top and bottom reinforcing bar level at and away from the crack. The chloride contents were not determined for all the specimens as they were similar to other mixes. The macrocell current at the time of removal and the integrated macrocell current data are included. Note that the chloride levels at the lower bar level under the crack are lower for the TZD and X35 specimens, which will be addressed in detail when the chloride analyses at the end of testing are discussed.

Figure 16 shows the corrosion of the BB-2 specimen at 34 cycles. As both BB specimens had similar behavior only one is shown. There is some corrosion on the bottom bar that would account for the macrocell current decreasing in time as the bottom bar was both an anode and a cathode. The BB corroded in the first cycle so the chloride contents are well beyond the point of when corrosion initiated and much higher than the 500 to 600 ppm on concrete typically used for black bar.

TABLE 12 Acid soluble chloride contents (on concrete) and corrosion data at 34 cycles (36 for TZE)

Specimen	Potential (mV, CSE)	Absolute Current ($\mu A/cm^2$)	Coulombs	Bar	Chloride Value (crack)(ppm)	Chloride Value (offset) (ppm)
X35 - 3	-210	0.081	492	Top	2582	662
				Bottom	1247	493
X35 - 5	-352	0.754	2930	Top	2212	620
				Bottom	1085	732
SS - 1	-183	0.002	57	Top		
				Bottom		
SS - 5	-194	0.002	53	Top	2385	613
				Bottom	1676	571
TZE - 1	-371	0.160	190	Top	2070	669
				Bottom	1335	562
TZE - 5	-290	0.049	77	Top	2613	704
				Bottom	1548	587
TZD - 4	-391	2.374	1568	Top	2530	701
				Bottom	1478	692
TZD - 5	-204	0.023	586	Top	1944	939
				Bottom	686	497
EC - 1	-72	0.009	25	Top	2521	766
				Bottom	1611	510
EC - 5	-70	0.002	27	Top	2530	800
				Bottom	1458	746
HDG - 2	-450	0.024	372	Top	2778	779
				Bottom	1671	722
HDG - 4	-619	0.049	1139	Top		
				Bottom		
BB - 2	-408	0.523	3336	Top	2653	690
				Bottom	1668	728
BB - 5	-404	0.783	3432	Top		
				Bottom		

FIGURE 16 BB-2 bars after 34 cycles (68 weeks) of corrosion testing.

Figure 17 shows the TZD bars after removal at 34 cycles. One bar with a high macrocell current and high integrated current, TZD-4, shows corrosion damage. The bars in specimen TZD-5 had lower current and did not have red rust. No

red rust corrosion is evident on the bottom bars; however, about 2% white corrosion product is on one bottom bar. Chloride values at the reinforcing bar levels indicate that the acid soluble corrosion threshold for severe corrosion occurs between 1,400 and 2,500 ppm chloride based on mass of the concrete.

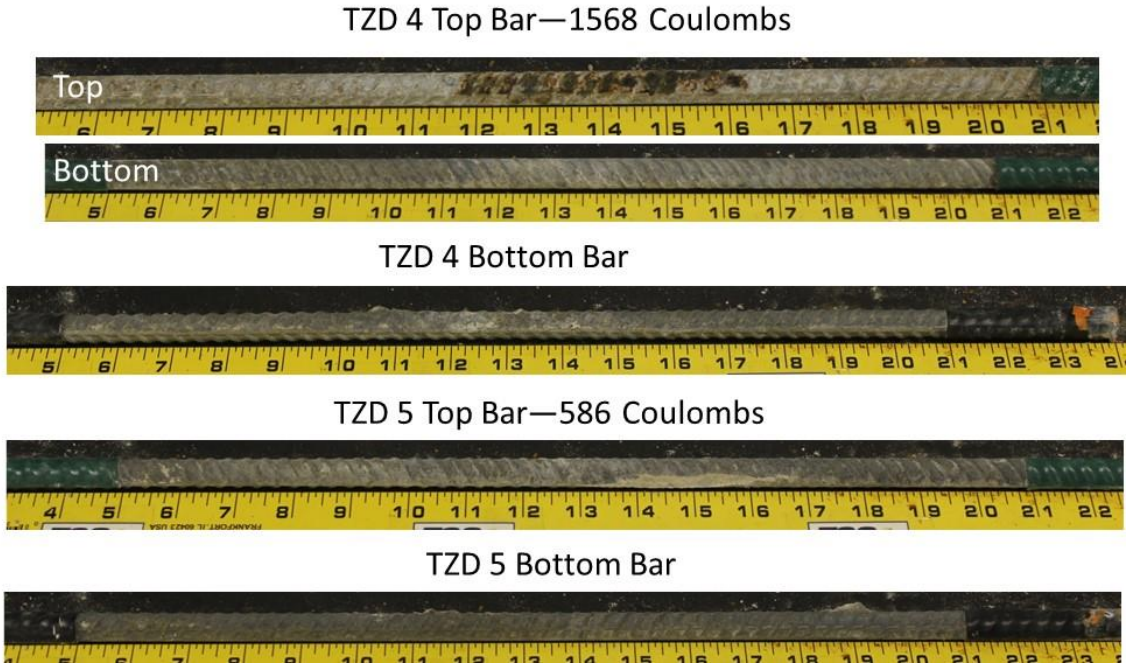

FIGURE 17 TZD bars after 34 cycles (68 weeks) of corrosion testing.

Figure 18 shows the HDG bars at 34 cycles. Though the corrosion macrocell currents were low on the HDG-2 bars there is evidence of white corrosion products on both the top and bottom bars and some rust spots on the top bar. The HDG-4 top bar has a deep pit and both bars show white corrosion products, typical of corroding zinc.

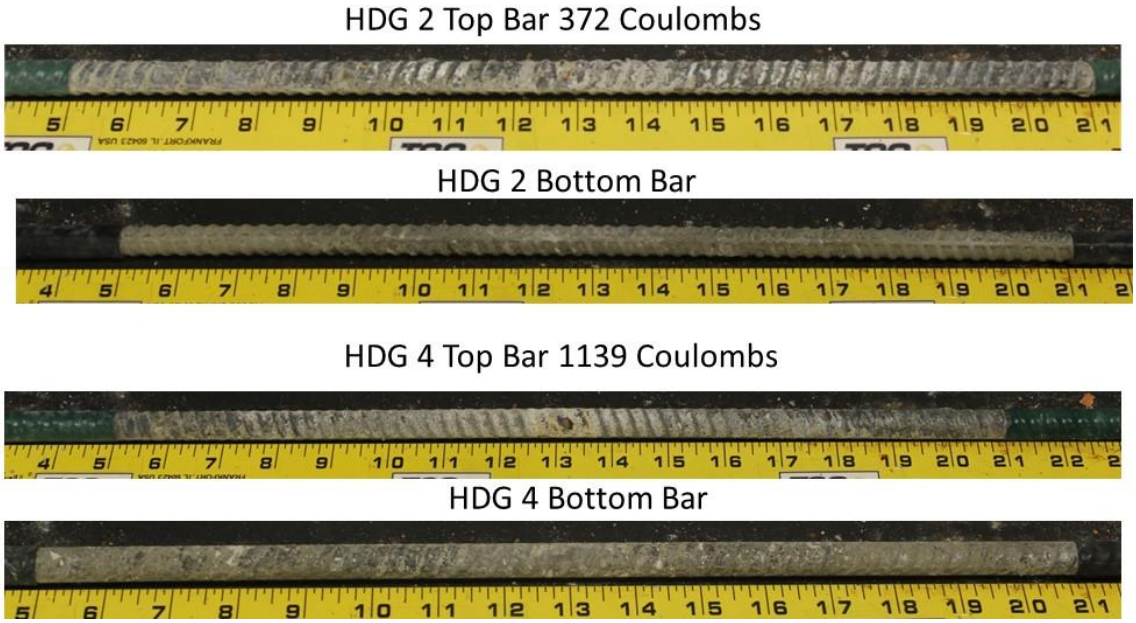

FIGURE 18 HDG bars after 34 cycles (68 weeks) of corrosion testing.

The chloride data in Table 12 indicate that the corrosion threshold would be under 2,500 ppm of chloride by mass of concrete. However, since corrosion occurred at lower macrocell activity this value is most likely lower, and bottom bar corrosion indicates that the threshold is less than 1,600 ppm of chloride. Analysis of chloride threshold for TZD and HDG is complicated by the pre-passivation high corrosion rate followed by a slow passive rate. Both bars far surpassed the performance of the BB, which had corrosion on the top and bottom bars and initiated corrosion early.

Figure 19 shows the X35 bars removed at 34 cycles. There was some corrosion on the bottom bars, but this is indicative of the original condition of some of the bars after wire brushing off rust in the as-received condition (see Appendix), the bottom bars at 52 cycles showed no rust. The chloride levels at the bottom bars were over 1,335 ppm and the top bars were over 2,200 ppm, indicating that the chloride threshold is over 1,400 ppm but less than 2,200 ppm.

FIGURE 19 X35 bars after 34 cycles (68 weeks) of corrosion testing.

Figure 20 shows the ECR and SS bars. There no sign of corrosion on the ECR at that time. The SS bar had one rust stain (arrow) but otherwise was in excellent condition. Concrete did not stick to either of these steels, unlike the case for the other bars.

The chloride data would indicate that the chloride threshold value is greater than 2,400 ppm by mass of concrete for the SS bar. Since there were no coating defects on the ECR, it performed well in the accelerated testing up to 34 cycles. Rapid ingress of chlorides might not provide sufficient time for organic coating failure processes to occur so it is difficult to determine a chloride corrosion threshold.

The TZE bars after 36 cycles are shown in Figures 21 and 22. The hand-painted coating had poor adhesion and rubbed off during the fabrication of the minibeams. Since there is slightly more damage in the middle of the bars, the fatigue cycling might have caused some of the damage. Even with the coating compromised, there was only slight rust staining on the top bar in Specimen 1. The visual performance was better than BB and TZD and HDG even with the poor coating.

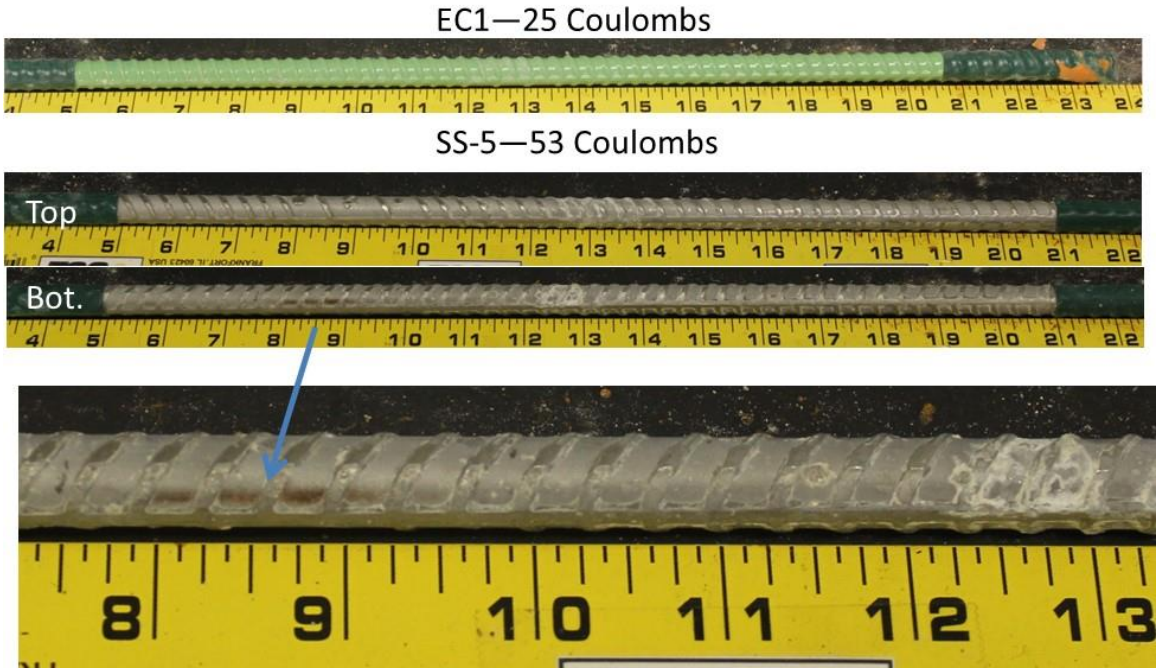

FIGURE 20 ECR and SS bars after 34 cycles (68 weeks) of corrosion testing. Arrow shows staining on SS bar.

FIGURE 21 TZE-1 bars after 36 cycles (72 weeks) of corrosion testing.

FIGURE 22 TZE-4 bars after 36 cycles (72 weeks) of corrosion testing.

At the end of testing, 52 cycles (104 weeks), complete autopsies were completed on the remaining groups of specimens. Table 13 shows the average chloride profiles at and away from the cracks and at the bottom bars. A statistical analysis (n = 3) showed that at an 80% Confidence Limit, there was a reduction of mean chloride concentration at the bottom rebar level under the crack for the TZD versus BB minibeams with a confidence limit of $\pm$150 ppm by mass of concrete.

TABLE 13 Average acid soluble chloride (on concrete) profiles for specimens removed after 52 cycles (two years) of testing

Beam Rebar	Sample Location	Depth Increments in Inches				
		0 to 1/2	1/2 to 1	1 to 1-1/2	1-1/2 to 2	2 to 2-1/2
BB	1- Top Center Crack	5662	4052	3226	2976	2251
	2- Top Offset	4039	1778	639	891	650
	3- Bottom Center Crack			1600		
	4- Bottom Offset			901		
HDG	1- Top Center Crack	6394	4010	3574	2861	3058
	2- Top Offset	3944	1648	828	735	700
	3- Bottom Center Crack			1635		
	4- Bottom Offset			652		
TZD	1- Top Center Crack	6312	4364	3326	2823	2580
	2- Top Offset	4214	1802	771	688	824
	3- Bottom Center Crack			1296		
	4- Bottom Offset			668		
X-35	1- Top Center Crack	5434	3586	2940	2709	2232
	2- Top Offset	3646	1479	841	688	767
	3- Bottom Center Crack			1498		
	4- Bottom Offset			688		
EC	1- Top Center Crack	6389	3946	3295	2825	2567
	2- Top Offset	3669	1787	869	815	800
	3- Bottom Center Crack			1565		
	4- Bottom Offset			798		
SS	1- Top Center Crack	5844	3872	3139	2721	2523
	2- Top Offset	2913	1500	830	777	791
	3- Bottom Center Crack			1793		
	4- Bottom Offset			637		
TZE	1- Top Center Crack	5818	3751	3305	2890	2687
	2- Top Offset	3907	1669	720	621	650
	3- Bottom Center Crack			1840		
	4- Bottom Offset			776		

As expected, the chloride levels at the cracks were considerably higher than away from the cracks in the top 2.5 in. of the specimens. The increase in chloride 5 in. from the surface under the crack (as indicated by comparing "Bottom Center Crack" with "Bottom Offset" values in Table 13) was unexpected and indicates that surface crack could potentially affect bottom mat reinforcing bars.

The chloride levels at 52 cycles were higher than at 34–36 cycles as expected. Only the SS bars had no corrosion at 52 cycles so their chloride threshold value in this test would be over 2,700 ppm by mass of concrete or 10.7 pcy. The value for the X35 remains at 7.9 pcy as found at 34 cycles. The X35 most likely would have had better performance if it had a cleaner initial surface. The TZD and HDG bars would still have a range of performance as it is not as clear as to when they started to corrode. This is especially true for the HDG bars. All bars outperformed the BB.

Analysis of the bars at the completion of testing adds considerably more information. Photographic, metallography, and mass loss tests were performed to compare the corrosion of the bars to the macrocell measurements. This is useful in determining if the macrocell data did not account for all of the corrosion (due to microcells and bottom bar corrosion) and to see how the bars perform after corrosion initiated.

Figures 23–29 show representative bars after 52 cycles at the completion of the corrosion testing. The top bar designated 1 and the two bottom mat bars designated as 2 and 3 are shown. The summary of the corrosion damage for the bars at 34 (36 cycles TZE) and 52 cycles is shown in Table 14. Table 15 shows the statistical analysis of the results when the percentage of rust based on surface area is multiplied by the degree of rust. Most weight is given to pitting corrosion where the corrosion was on the order of or higher than the rib height. The visual rating system is shown in Figure 30.

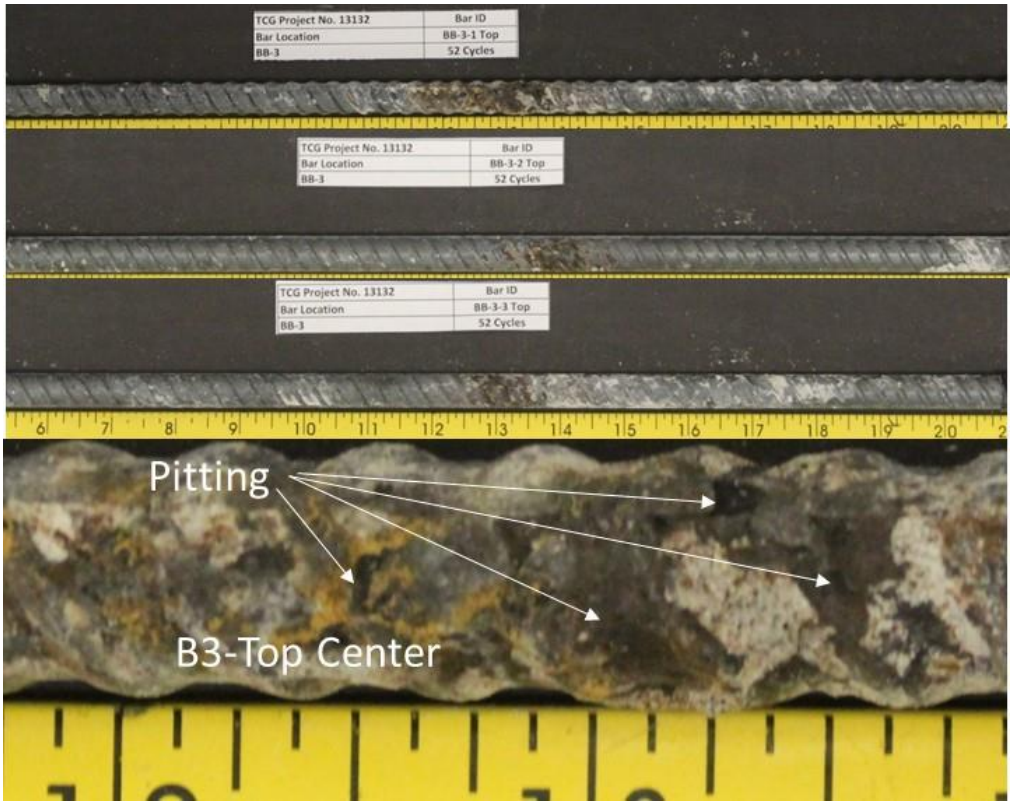

FIGURE 23 BB-3 bars after 52 cycles. Bar 1 is the top bar and bars 2 and 3 are the bottom mat bars.

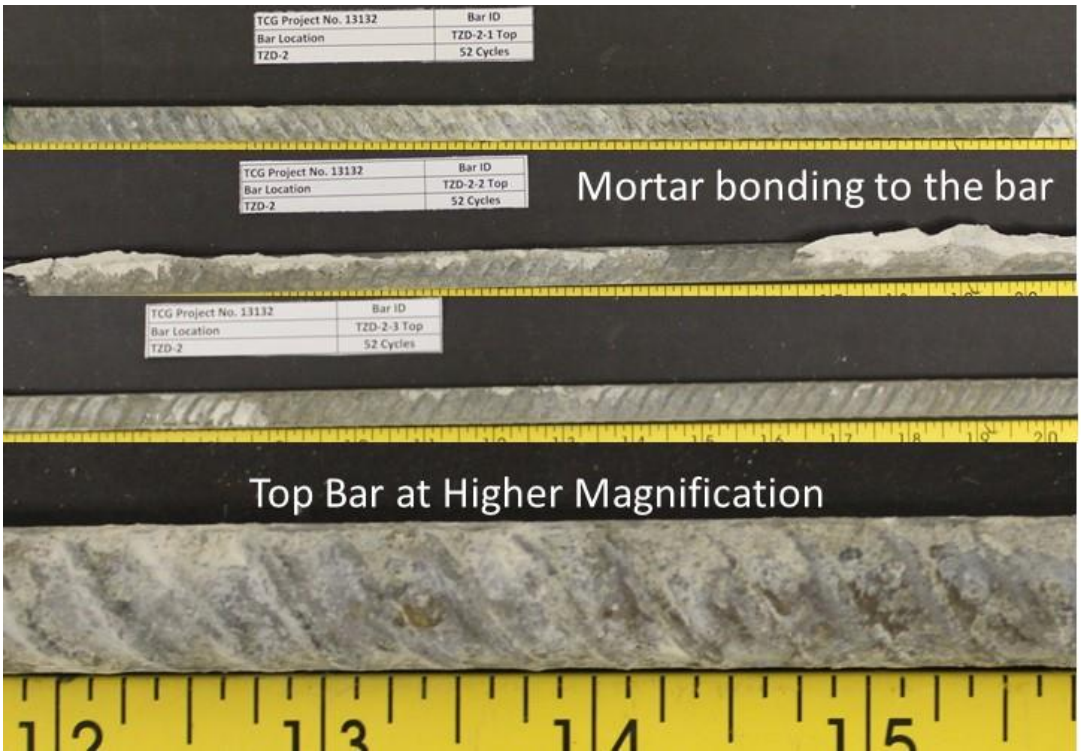

FIGURE 24 TZD-2 bars after 52 cycles. Bar 1 is the top bar and bars 2 and 3 are the bottom mat bars.

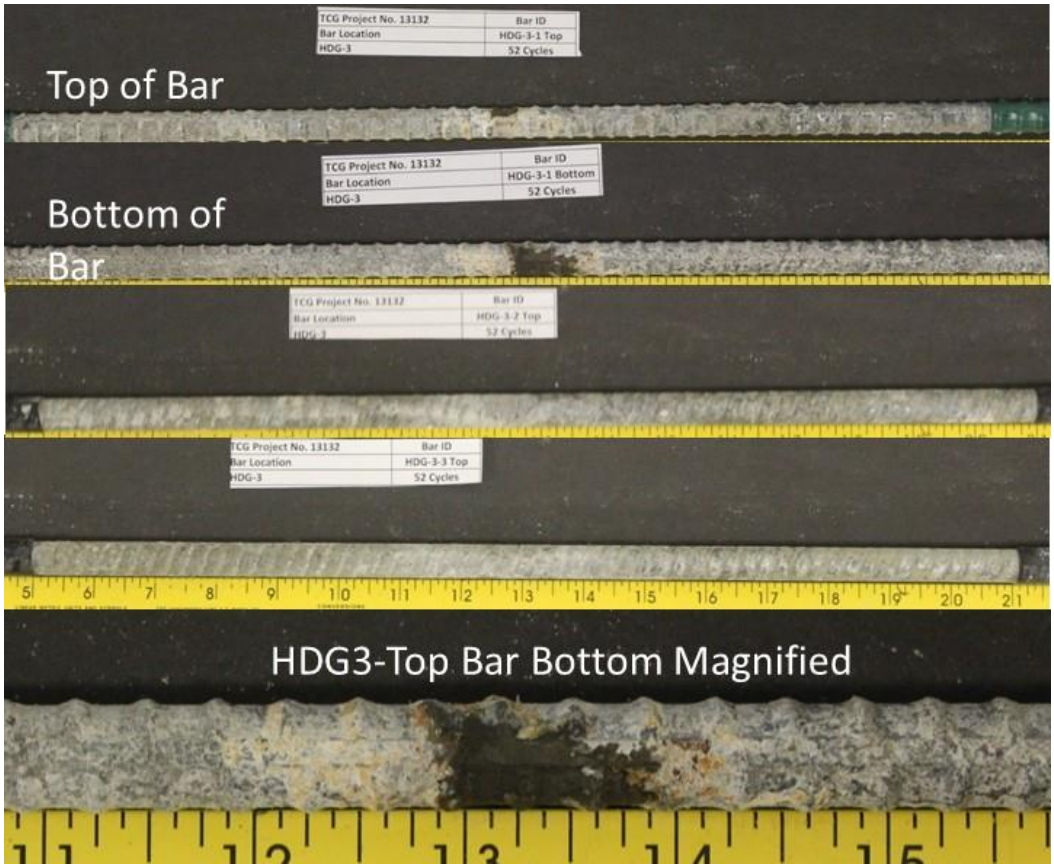

FIGURE 25 HDG-3 bars after 52 cycles. Bar 1 is the top bar and bars 2 and 3 are the bottom mat bars.

FIGURE 26 TZE-2 bars after 52 cycles. Bar 1 is the top bar and bar 2 is a bottom mat bar.

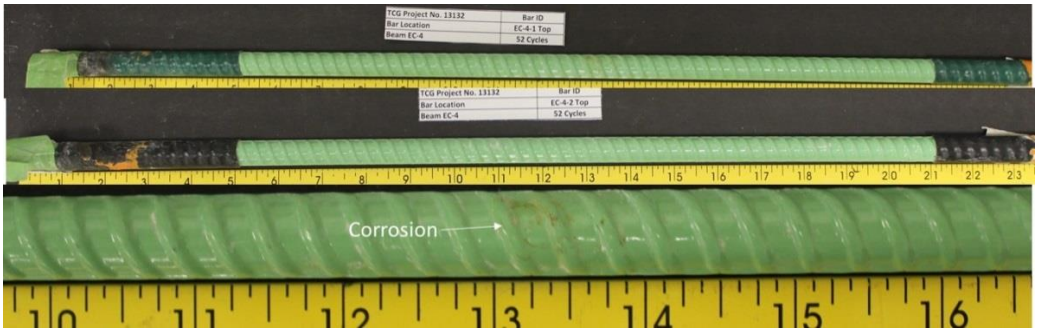

FIGURE 27 ECR-4 bars after 52 cycles. Bar 1 on top and magnified or the top bar, bar 2 is a bottom mat bar.

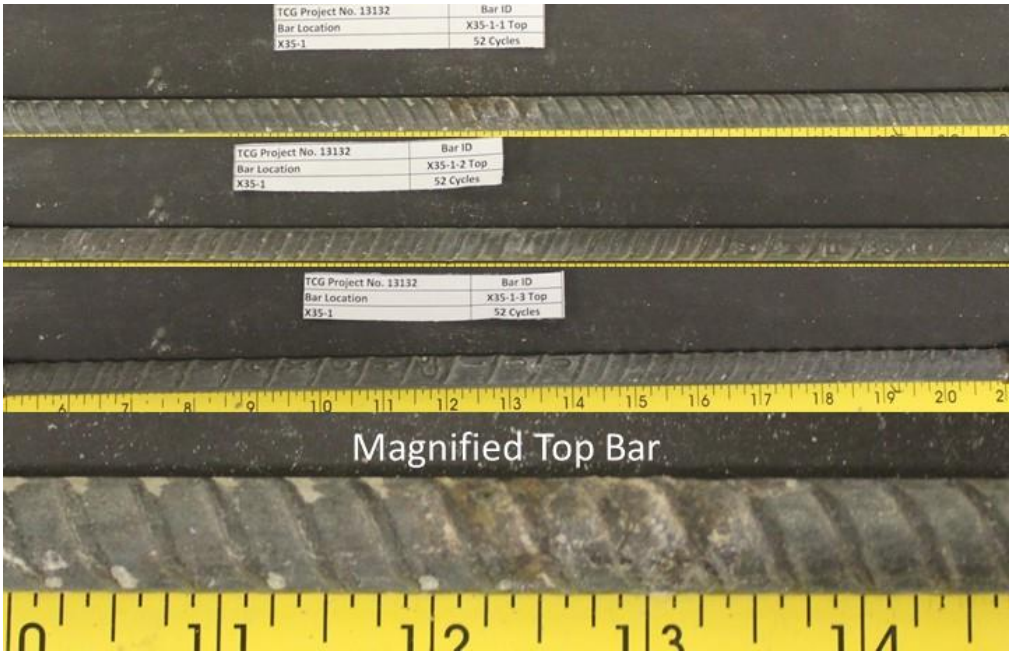

FIGURE 28 X35-1 bars after 52 weeks of corrosion. Bar 1 is the top bar and bars 2 and 3 are the bottom mat bars.

FIGURE 29 SS-3 bars after 52 cycles. Bar 1 is the top bar and bar 2 is a bottom mat bar.

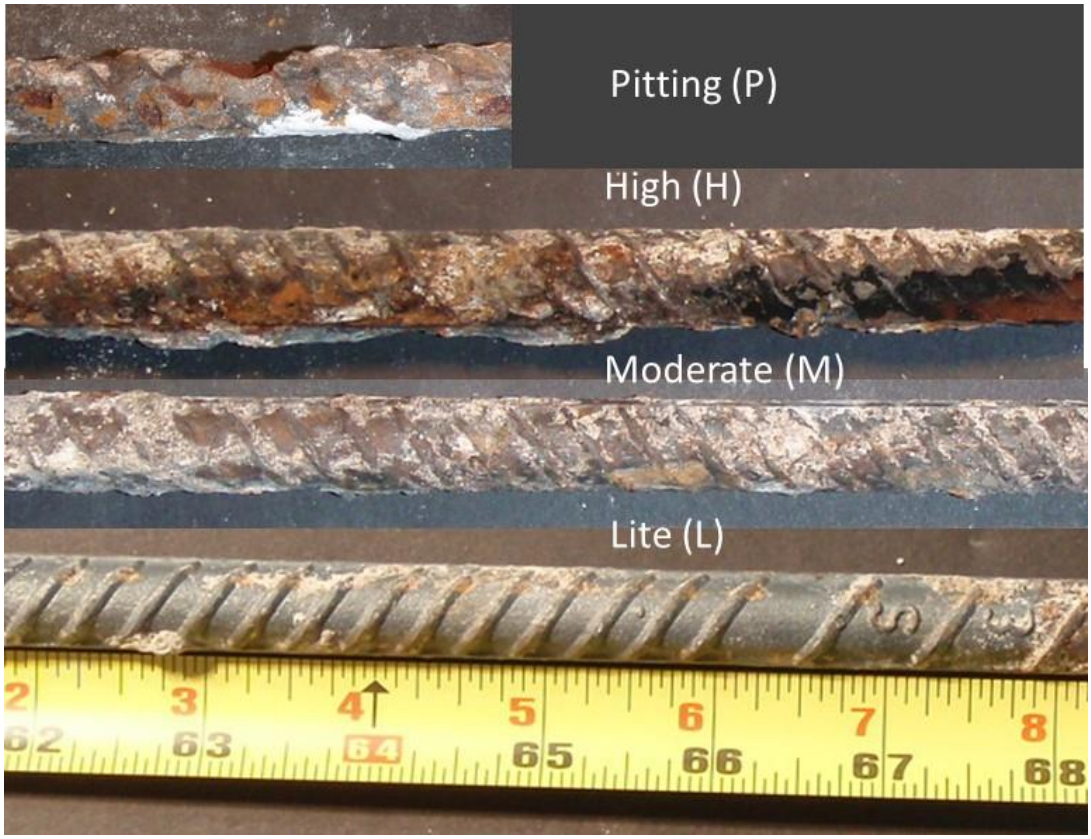

FIGURE 30 Visual rating system for corrosion performance used in Tables 14 and 15.

TABLE 14 Summary of visual corrosion damage and integrated macrocell current at 34 and 52 cycles (1 cycle = 2 weeks)

Bar	Beam #	Cycles at Removal	% Red Rust			% White Rust			Corrosion Severity			Coulombs at Removal
			Bar 1	Bar 2	Bar 3	Bar 1	Bar 2	Bar 3	Bar 1	Bar 2	Bar 3	
BB	1	52	4	3	3				P	M	M	2523
	2	34	3	3	3				P	M	M-H	3336
	3	52	4	3	3				P	M	M	2182
	4	52	4	3	0				H-P	L-M	0	3495
	5	34	4	3	3				P	M	H	3432
HDG	1	52	5	1	2	4	1	2	L	L	L	4523
	2	34	3	0	0	3	3	4	M	L	L	112
	3	52	3	3	2	3	3	2	H-P	L	L	576
	4	34	3	2	0	5	4	5	M	L	L	1139
	5	52	4	4	3	4	3	2	H	L	L	276
TZE	1	36	3	2	0				L	L	-	186
	2	52	4	1	0				M	L	-	210
	3	52	3	1	0				M	L	-	154
	4	52	2	0	0				L	-	-	101
	5	36	3	0	0				L	-	-	76
TZD	1	52	3	0	0	3	3	3	M	L	L	4174
	2	52	3	0	0	3	0	2	L	-	L	859
	3	52	1	0	0	4	0	4	L	-	L	771
	4	34	3	0	0	3	0	2	M	-	-	1568
	5	34	0	0	0	1	0	0	L	-	-	585
X35	1	52	3	2	0				L-M	L	-	2428
	2	52	3	0	0				L-M	-	-	1657
	3	34	3	4	4				H	L	L	492
	4	52	4	1	0				M-H	L	-	2407
	5	34	3	4	4				H	L	L	2930
SS	1	34	0	0	0				-	-	-	46
	2	52	0	0	0				-	-	-	49
	3	52	0	0	0				-	-	-	50
	4	52	0	0	0				-	-	-	44
	5	34	0	0	0				-	-	-	29
ECR	1	34	0	0	0				-	-	-	20
	2	52	1	0	0				L	-	-	26
	3	52	0	0	0				-	-	-	22
	4	52	2	0	1				L	-	L	34
	5	34	0	0	0				-	-	-	14

L=Light corrosion product

M=Moderate corrosion product

H=High corrosion product

P=Pitting and loss of steel

Note: White rust is applicable to zinc coated bars only.

TABLE 15 Statistical analysis of data in Table 14. Corrosion damage is % red rust *severity

Bar	Cycles at Removal	Stats	% White Rust		Corrosion Damage (%RR*M) Multiplier L=1; M=3;H=5;P=10		Coulombs
			Bar A	Bottom Bars	Bar A	Bottom Bars	
BB	34	Mean	Not Applicable		35.0	11.3	3384
		Std.Dev.			5.0	2.5	48
	52	Mean			36.7	7.0	2733
		Std.Dev.			4.7	3.3	556
HDG	34	Mean	4.0	4.0	9.0	0.5	626
		Std.Dev.	1.0	0.5	0.0	0.9	514
	52	Mean	3.7	2.5	12.3	2.5	1792
		Std.Dev.	0.8	0.8	2.9	0.8	1743
TZE	34	Mean	Not Applicable		3.0	0.5	131
		Std.Dev.			0.0	0.9	55
	52	Mean			7.7	0.3	155
		Std.Dev.			3.1	0.5	35
TZD	34	Mean	2.0	0.5	4.5	0.0	1077
		Std.Dev.	1.0	0.9	4.5	0.0	492
	52	Mean	3.3	2.0	4.3	0.0	1935
		Std.Dev.	0.5	1.5	3.4	0.0	1584
X35	34	Mean	Not Applicable		15.0	4.0	1711
		Std.Dev.			0.0	0.0	1219
	52	Mean			9.3	0.5	2164
		Std.Dev.			4.7	0.8	359
ECR	34	Mean			0.0	0.0	17
		Std.Dev.			0.0	0.0	3
	52	Mean			1.0	0.0	27
		Std.Dev.			0.9	0.0	6
SS	34	Mean			No Rust		38
		Std.Dev.					9
	52	Mean					48
		Std.Dev.					3

The corrosion data in Table 15 is shown in Figures 31 and 32. Figure 31 shows that all the bars are outperforming BB at both 34 (36 for TZE) and 52 cycles. The SS bars are not included as they did not show visual corrosion other than a light stain on one bar at 34 cycles. The 52-week data are not always more severe than the 34-cycle data as the highest and lowest corroding minibeams were removed at 34 cycles and the more corroding beam influenced the results. For the top bars, this was true for the X35 specimens. At 52 cycles the visual performance for red rust would be in decreasing severity:

$$BB > HDG > X35 > TZE \approx TZD > ECR > SS.$$

There was significantly more corrosion on the BB bottom bars than on the other specimens.

The white rust was only applicable to TZD and HDG and consists of zinc corrosion products. As can be seen in Figure 32 the white rust was similar between TZD and HDG bars. Based on macrocell currents alone, HDG would have been expected to be better than both the TZD and X35 bars. However, the bottom mat was a poorer cathode, as would be expected being a purer zinc than TZD and not a steel alloy or iron-zinc intermetallic, and in addition, HDG bottom bars went into corrosion, further limiting the cathodic current they could supply to the top mat.

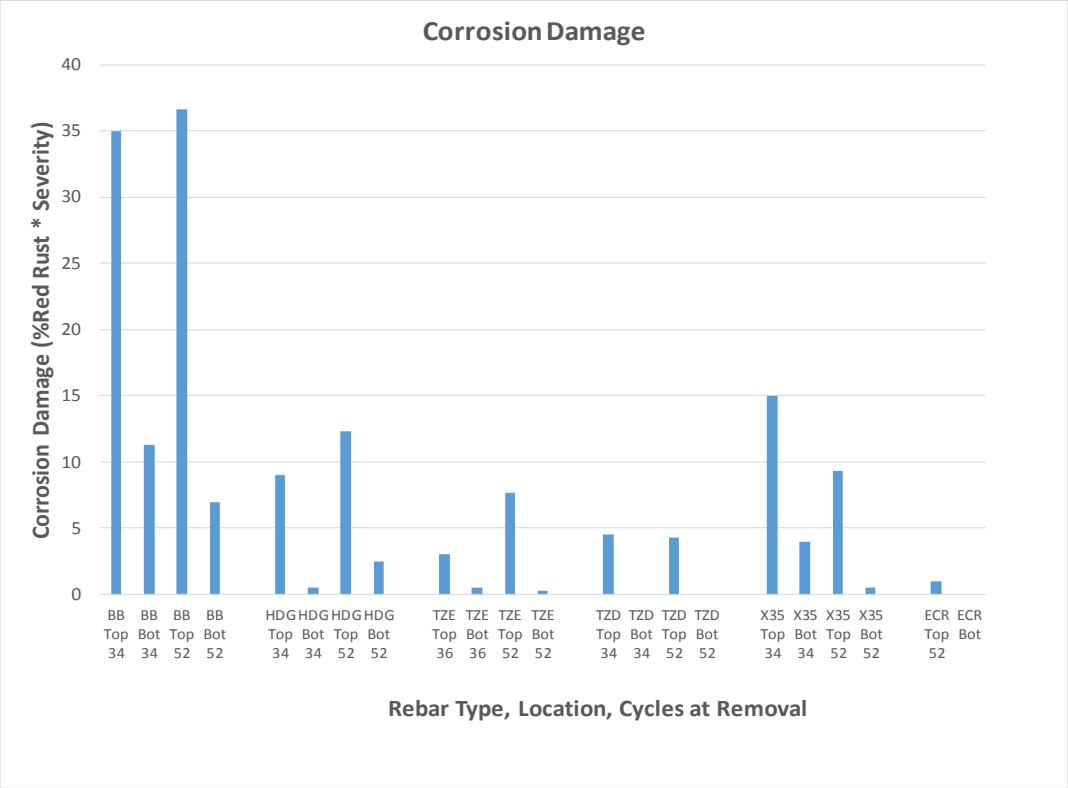

FIGURE 31 Corrosion of reinforcing bars at the completion of testing. SS bars had no visual rust.

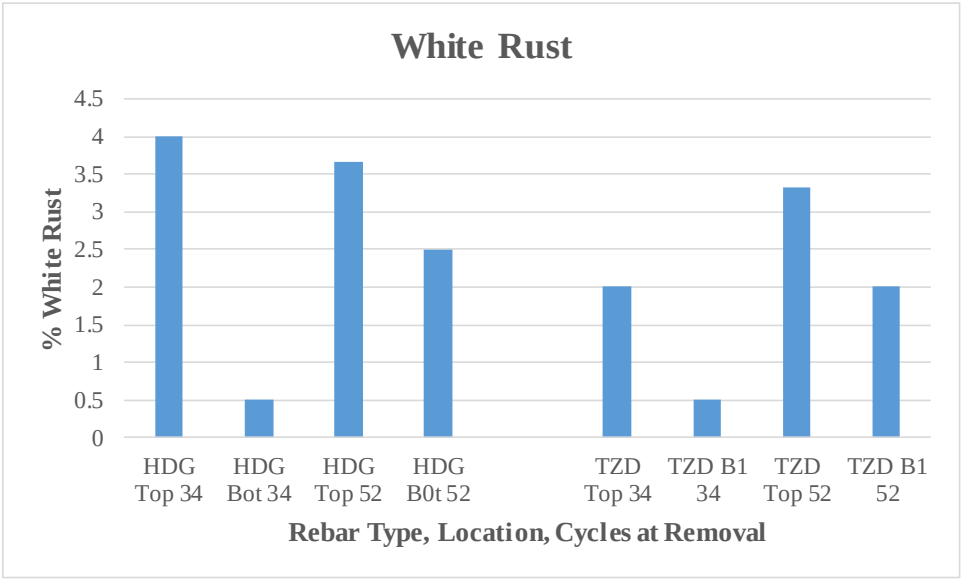

FIGURE 32 White rust on TZD and HDG bars at the completion of testing.

The last series of tests was mass loss conducted on sections of some bars after removal and comparing it with the initial masses per unit length of non-corroded bars. This testing was performed for the uncoated bars and the TZD and HDG bars.

Removing the epoxy coatings without damaging the substrate would require hazardous organic solvents, so it was not performed, given the negligible corrosion on these bars. Bars were cleaned with a bristle brush before chemically stripping the corrosion products using concentrated acid solution stipulated in ASTM G1. BB was cleaned with solution C.3.5 [500 mL hydrochloric acid (HCl, sp. Gr. 1.19) 3.5 g hexamethylene tetramine, Reagent water to make 1000 mL], SS and X35 were cleaned with solution C.7.1. (100 mL nitric acid (HNO_3, sp. Gr. 1.42), Reagent water to make 1000 mL) Initial coating thickness for TZD and HDG were determined by dissolving the zinc coatings in C.3.5. After completion of testing, the corrosion products were removed from the TZD and HDG coatings using solution C.9.5 [100 g ammonium persulfate ($(NH_4)_2S_2O_8$), Reagent water to make 1000 mL] and then the remaining zinc was determined by dissolving it off in the C.3.5 solution.

Table 16 has the calculated bar or coating loss for selected specimens. Also included is the total macrocell current divided by the entire area of the bar and then the calculated thickness loss based on Faraday's equation, shown below, relating mass loss to charge passed per unit area and dividing by the density to determine a thickness loss.

$$W = \frac{I * t * A}{n * F}$$

Where *W* is the weight of the plated metal in grams,

I is the current in coulombs per second,

t is the time in seconds,

A is the atomic weight of the metal in grams per mole,

n is the valence of the dissolved metal in solution in equivalents per mole,

F is the Faraday's constant

TABLE 16 Measured thickness losses and calculated average thickness loss (mils) based on the macrocell current/bar area

Rebar-Beam	Top Bar			Bottom Bar			Total Macrocell	Total Macrocell
	Near Rust*	No Rust	White Rust	Near Rust	No Rust	White Rust	C/cm^2	mils
BB-1	2.98	0.00		2.22	0.47		24.90	0.36
TZD-2	1.61	0.16	1.55		1.79	1.81	8.48	0.14
HDG-5	1.58	2.15	1.33	1.03	1.23	0.32	2.72	0.05
X35-1	1.29	0.00		0.32	0.19		23.97	0.35
SS-1	0.00	0.00		0.00	0.00		0.45	0.01

*Rust for uncoated bars, coating loss near rust location for coated bars.

The average thickness loss from the macrocell data is less than that measured in regions of high corrosion. This is to be expected as the corroding areas would have had higher current densities and only represent a small portion of the total area as seen in Table 14. The microcell corrosion could be appreciable [7] especially in the case of the HDG bars that showed reverse macrocells. Macrocell current is still a good indicator of corrosion activity but needs to be augmented with additional analyses as performed in this work. Based on macrocell alone times to corrosion induced cracking would be based on the total macrocell mils divided into 1 mil times 2 years; for example, about 5.5 years for the BB-1 specimen, assuming the average corrosion rate did not change.

3.3.2 U-Bends

Corrosion potential, polarization resistance (corrosion rate), electrochemical impedance spectroscopy (EIS, corrosion, resistivity), appearance, and chloride distributions were measured over a two-year period. Two of five specimens were removed at 68 weeks unless otherwise noted. The EIS was mainly used to determine the concrete resistivity between the reference electrode and the bar so that the polarization resistance could be corrected for the voltage drop due to passing current through a resistive medium (concrete), known as IR drop. This needed to be used as the U-bend configuration made it difficult for the potentiostat to correct for this automatically. The two methods have been shown to provide equal results [8].

Figure 33 shows the average corrosion potentials versus the saturated Calomel (SCE) reference electrode. ASTM G3 notes that the values would be approximately 60 mV more negative if a saturated $Cu/CuSO_4$ (CSE) was used. The HDG specimens seemed to have a less negative potential than found in the cracked minibeams and less negative than would be expected. There was a fair amount of variability that was presumably due to the low concrete cover and higher w/c for the concrete.

Figure 34 shows the average corrosion damage as the integration of the inverse of the polarization resistance, $1/R_p$ versus time. Initially, all of the specimens outperformed the BB but by 1 year the TZD specimens started to show high corrosion rates. The X35, HDG, and TZE continued to show an improvement, and the ECR and SS specimens showed the least corrosion behavior.

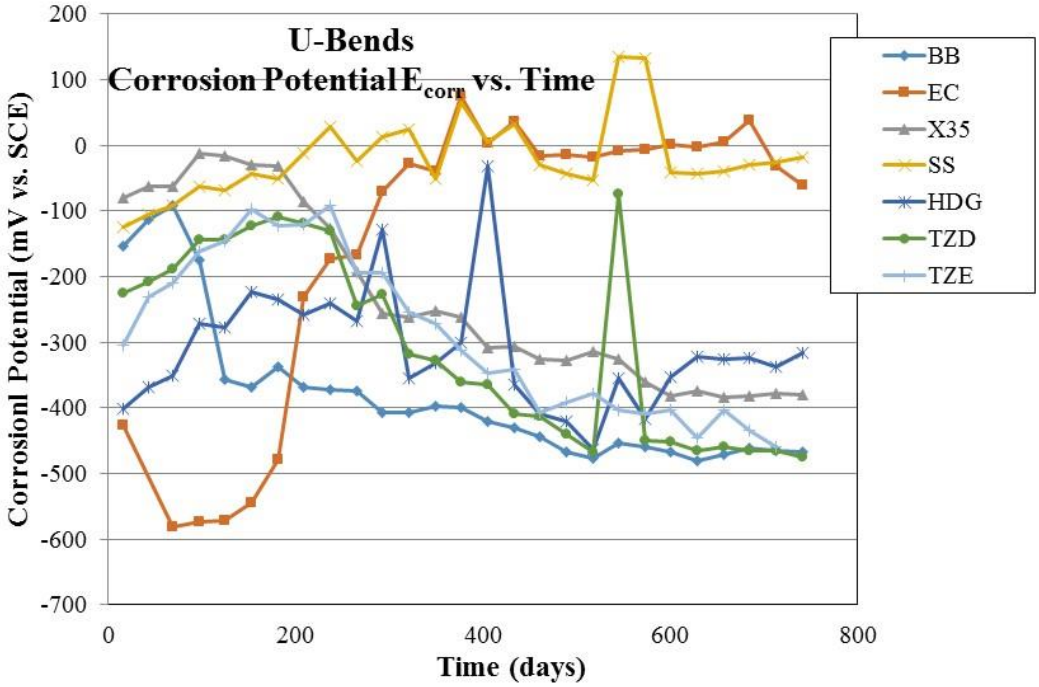

FIGURE 33 Average corrosion potentials versus time for U-bend specimens.

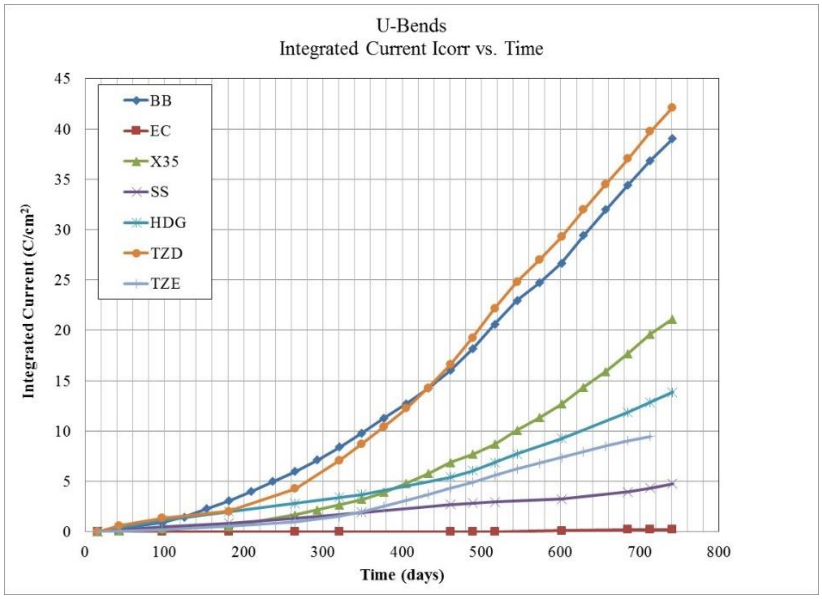

FIGURE 34 Total average corrosion versus time as measured by the integration of $1/R_p$.

The corrosion potentials for TZE and X35 became more negative as the corrosion started to decrease; this will be more clearly seen in the following graphs of the individual specimens.

Figure 35 shows the individual BB control specimens. The initial corrosion rate decreased until severe corrosion initiated, as seen in a large drop in potentials and an increase in 1/*Rp*; a calculated corrosion rate can be determined assuming a constant of 26 mV to multiply $1/R_p$. Assuming that 1 mil of average corrosion is needed to crack concrete the value would be approximately 68 C/cm^2 of integrated current [9]. The corrosion data are close to that value.

As can be seen in Figure 35, the corrosion rate ($1/R_p$) and corrosion current (I_{corr}) curves mimic each other, since they are related by a common (assumed) factor. Subsequent graphs will only show the $1/R_p$ data. This eliminates assumptions about the constants used to convert the data to currents.

Figures 36 and 37 show the U-bend data for the TZD as compared to X35 specimens. There is much more scatter in the TZD specimens. In contrast to the cracked beam data the TZD is not showing improvements over BB. The 1/*Rp* value at 686 days appears to be an anomaly. The X35 specimens are outperforming the BB specimens. Both show that a drop in corrosion potential correlates to a rise in corrosion activity.

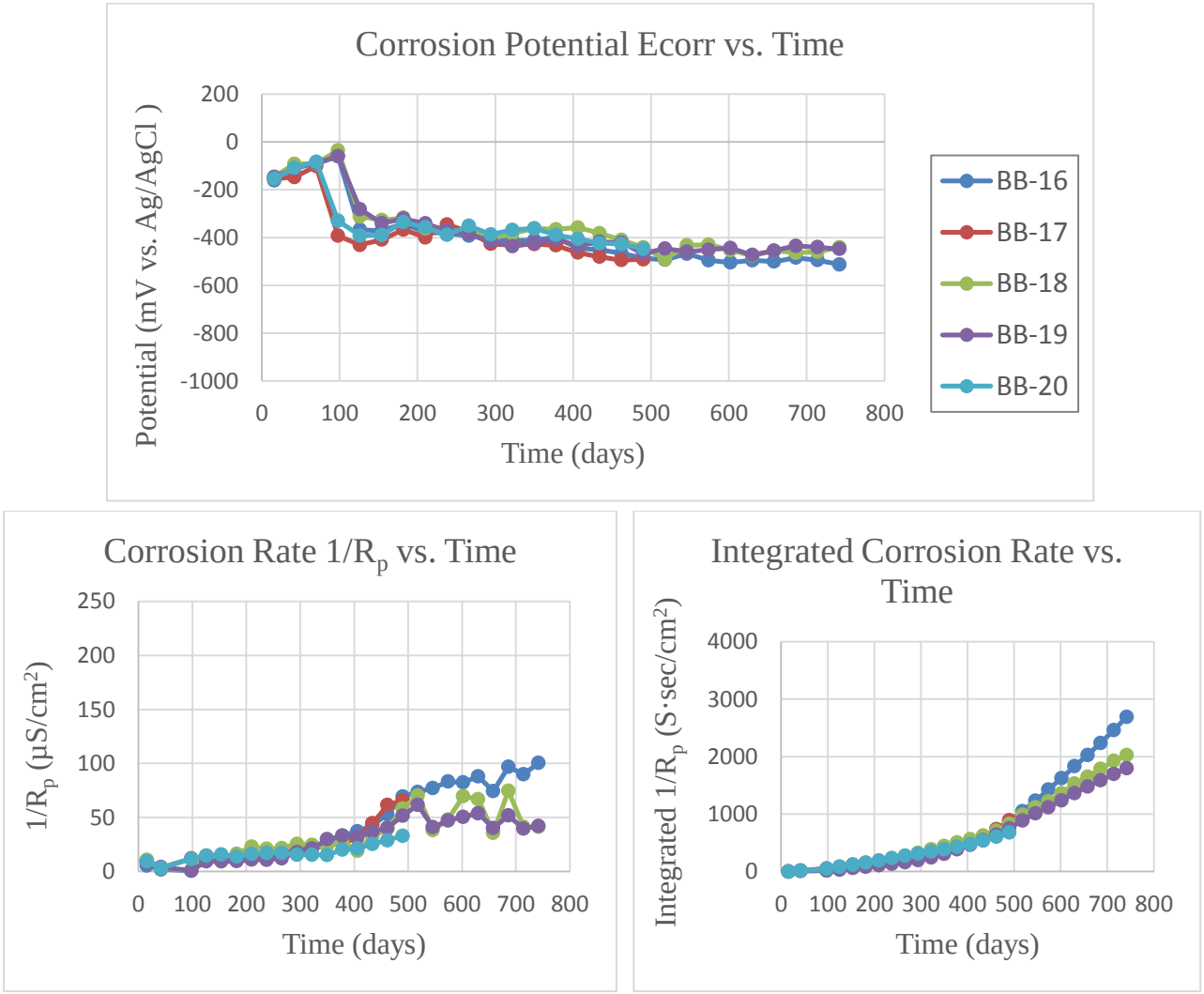

FIGURE 35 U-bend corrosion data over time for the BB specimens.

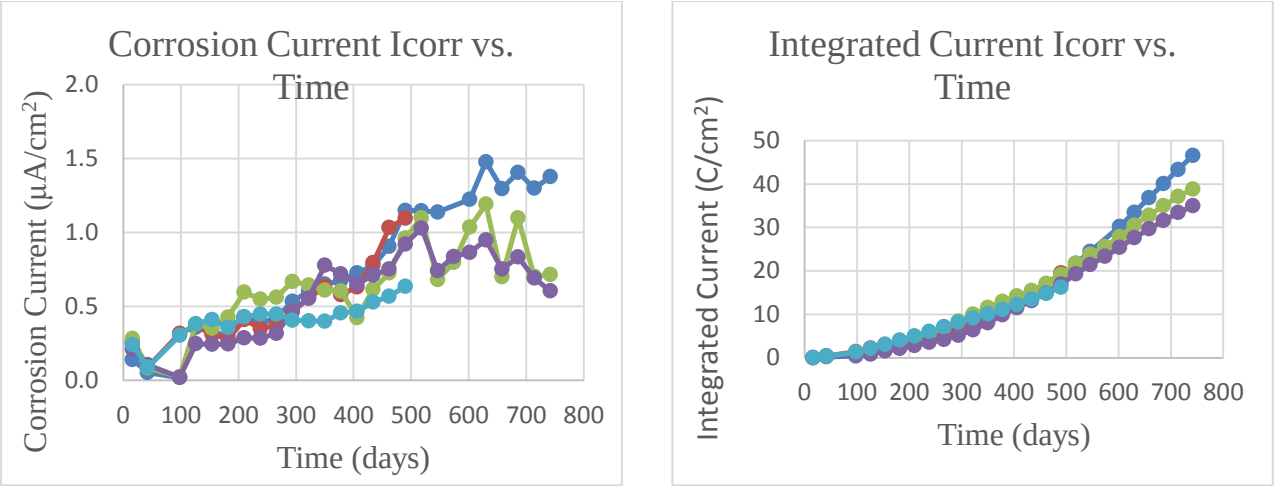

FIGURE 35 (cont.) U-bend corrosion data over time for the BB specimens.

Figures 38 and 39 show the results for HDG and TZE U-bend corrosion data. The HDG corrosion potentials are much more positive, even taking into account the -104 mV correction from SCE to CSE. The HDG specimens started to show an increase in corrosion rates at approximately 500 days indicating that the thicker zinc coating compared to TZD is starting to be lost. The TZE corrosion rates are lower even though, as seen in Figure 5, the coating had poor adhesion in the bends.

As noted earlier the stress was not released in the bend specimens as would be common practice, as a holder at the top was needed to keep the bar ends parallel to each other. This would adversely affect a more brittle intermetallic coating such as TZD, and cause poor adhesion for a non-optimized organic coating, which is reflected in the corrosion results.

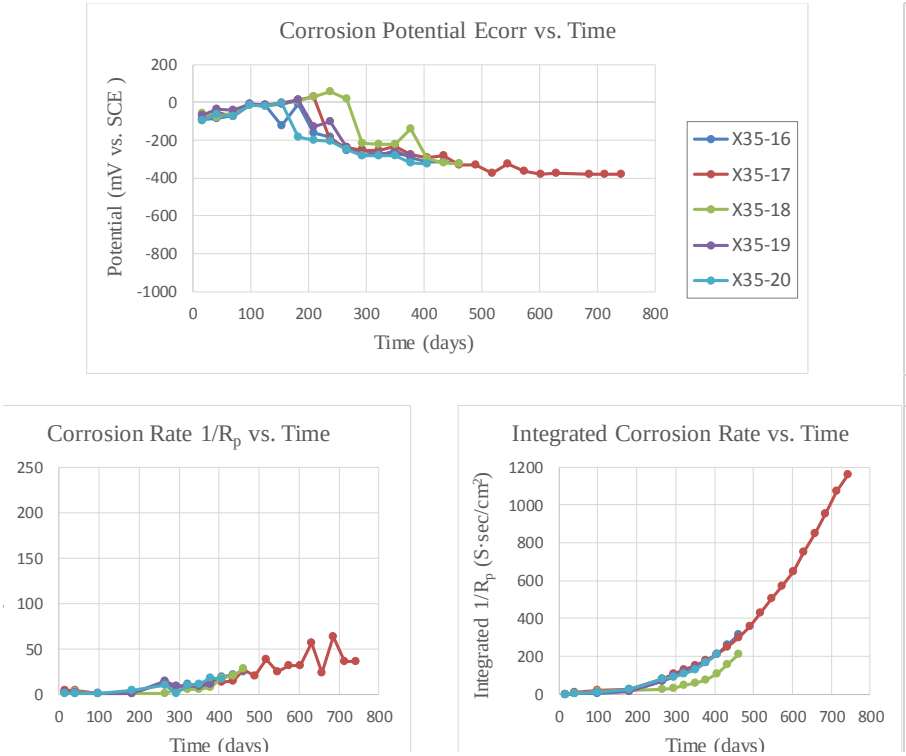

FIGURE 36 U-bend corrosion data for X35 specimens.

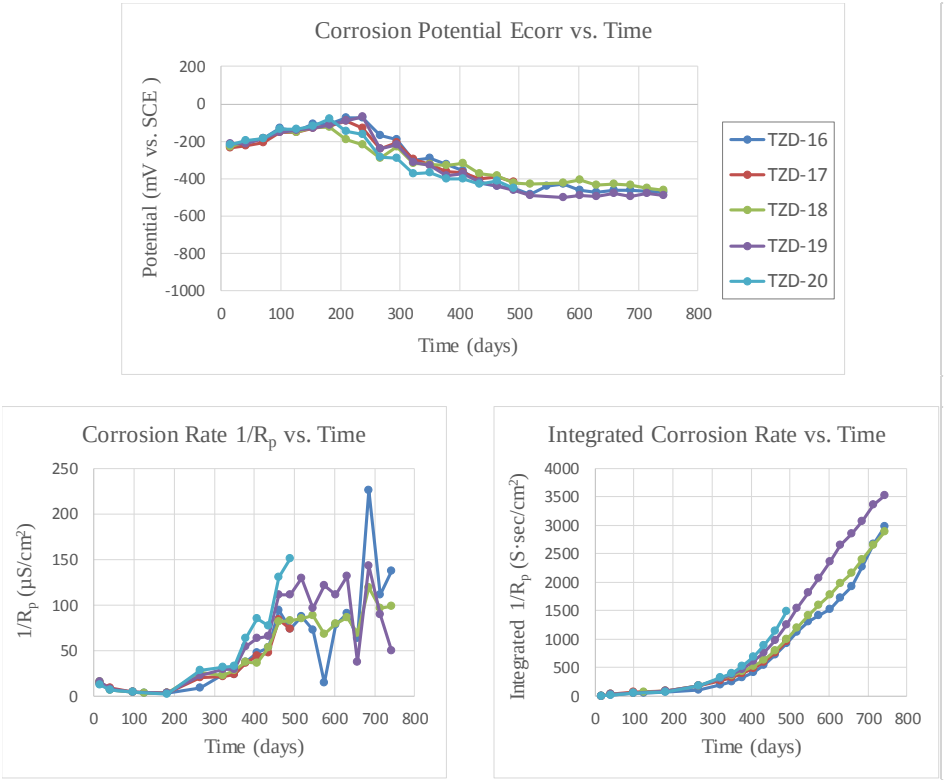

FIGURE 37 U-bend corrosion data for TZD specimens.

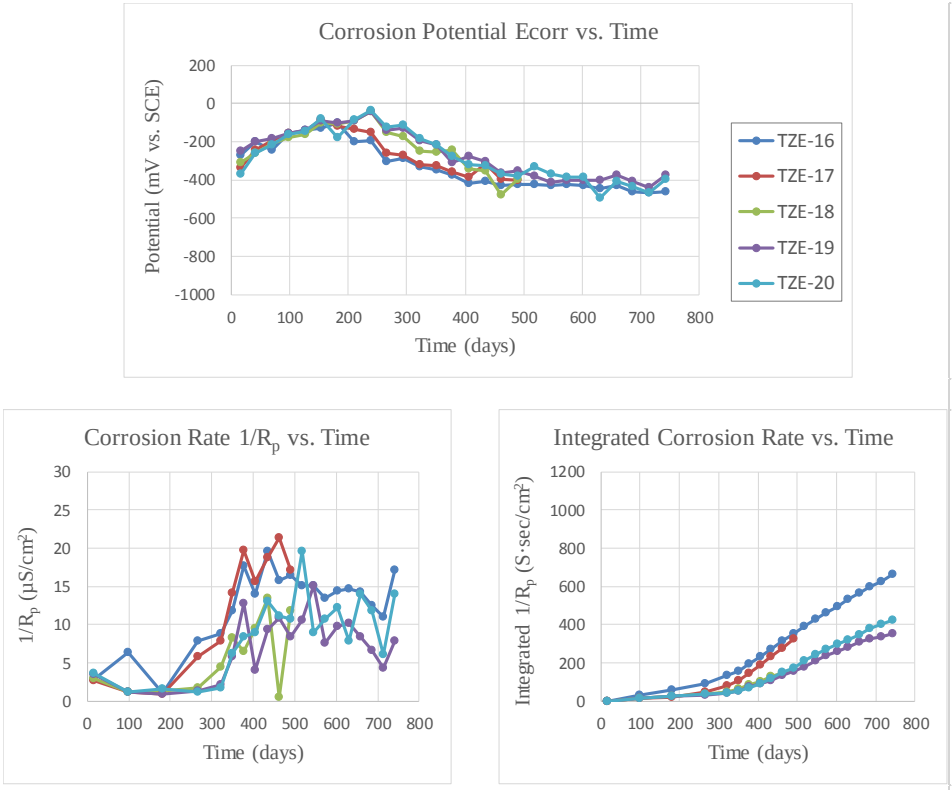

FIGURE 38 U-bend corrosion data for TZE specimens.

Figures 32 and 33 showed passive behavior for the SS and ECR U-bend specimens. As such the individual curves are not included. This is somewhat expected as the ECR coating, other than the initial bending, was not subjected to flexing or wetting and drying cycles at a flexed crack. For the SS specimens, the chloride ingress, as will be shown, did not exceed the experimentally determined chloride ion concentration threshold value.

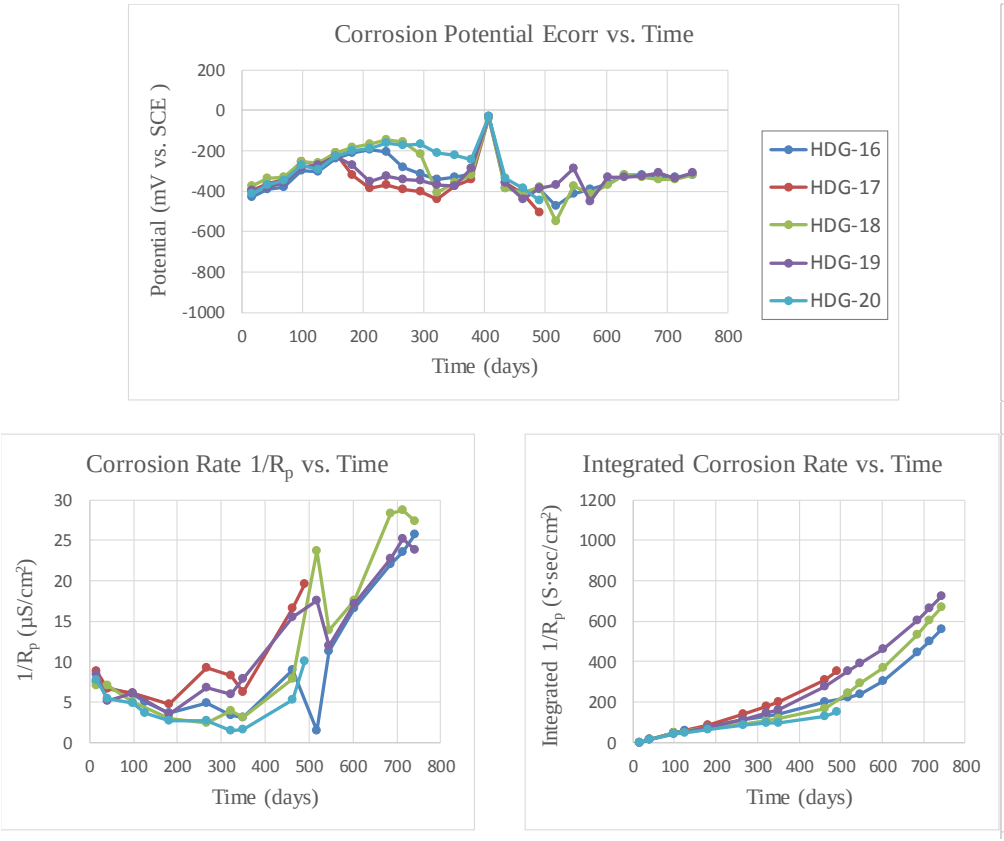

FIGURE 39 U-bend corrosion data for HDG Specimens.

Visual analysis of the specimens showed that all five BB specimens had severe corrosion staining and some cracking at the surface at 17 months (1.4 years of testing). Only one TZD specimen had small spots, and some HDG specimens showed some possible white corrosion products coming through. Figure 38 shows a comparison of a typical BB, HDG, and the one TZE with corrosion spots. The TZE, X35, SS, and ECR specimens did not show any corrosion on the surface. However, due to the calculated stresses on the X35 bars exceeding 90,000 psi a few of them broke when corrosion started, and the specimens were destroyed. Future testing would release the stress from bending or use a larger radius.

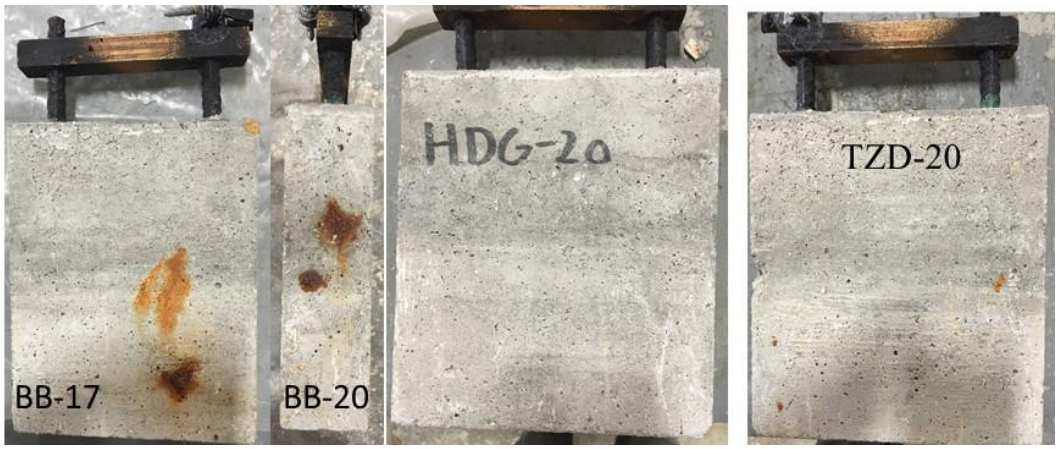

FIGURE 40 U-bend specimens after 1.4 years of corrosion testing.

The SS and ECR bars had no corrosion at that time and are not shown. The corrosion on the outside of the specimens in Figure 38 corresponds to the corrosion of the specimens in Figure 39. Visuals of U-bends are presented in Figure 42.

Chloride results for intermediate times and at the end of two years are in Figure 41. The chloride levels at the reinforcing bar level were in excess of 2,500 ppm (~10 lb Cl^-/yd^3 concrete) for all specimens except the HDG and ECR specimens. The chloride contents just above the 1-to-1.5-inch location of the bars were higher so this was a severe exposure.

Corrosion damage at the end of testing is given in Table 17. A similar analysis as used for the beam specimens was employed. The TZD was observed visually to outperform BB, in agreement with the surface corrosion damage. The corrosion damage of the TZE and HDG were similar. Given the higher stress (bars not relaxed and held in tension) than would be employed in the field, both still showed an improvement over the BB.

Photographs of typical corroding bars are shown in Figure 42. Though the area of rust on BB-18 was comparable to that on the other bars, it was more concentrated, resulting in pitting and the severe staining of the concrete surface. The degree of stress on the bars is evident in that they opened up from a U configuration upon removal of the clamp on the top (springback). This was most noticeable on the X35 bar since A1035 steel does not have a classic yield stress.

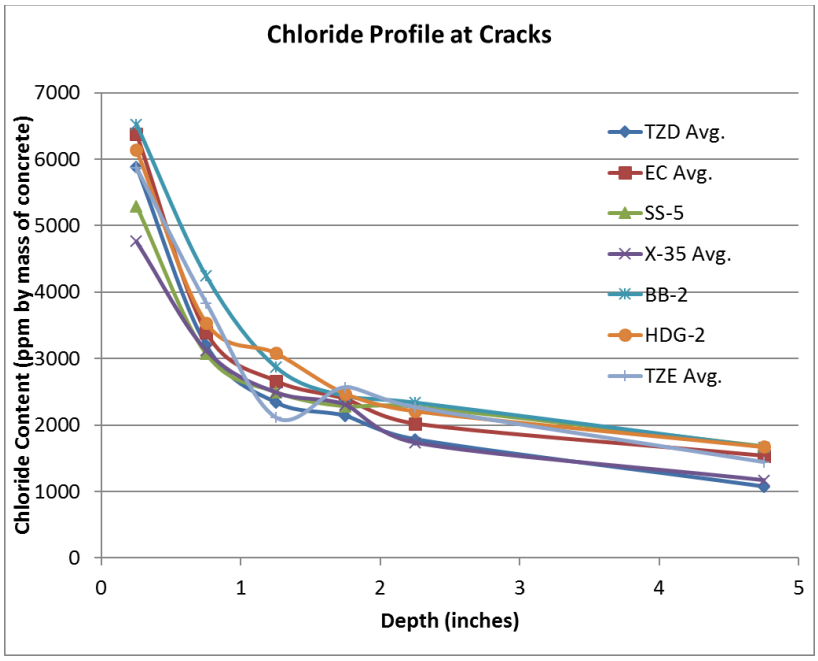

FIGURE 41 Chloride test results at the time of removal.

TABLE 17 Corrosion damage of U-beam bars

Mix	Beam #	Days at Removal	% Rust	% White Rust	Corrosion Severity (L=1,M=3,H=5,P=10		Corrosion Damage (%Rust*Severity)	Average Damage (at end)	Average % White Rust
			Bar A	Bar A	Rust	W Rust			
BB	16	754	5		H-P		37.5	38.3	
	17	476	4		P		40		
	18	754	4		P		40		
	19	754	5		H-P		37.5		
	20	476	3		M-H		12		
HDG	16	754	3	4	L-M	L	6	13.7	4.3
	17	476	4		H		20		
	18	754	5	5	M	L	15		
	19	754	5	4	M-H	L	20		
	20	476	1	1	L	L	1		
TZE	16	741	4		M-H		16	13.3	
	17	476	4		M		12		
	18	476	3		M		9		
	19	741	4		M		12		
	20	741	4		M		12		
TZD	16	754	4		H		20	23.3	
	17	476	4		H		20		
	18	754	5		H		25		
	19	754	5		H		25		
	20	476	5		H		25		
X35	17	754	3		H		15		

Note: The corrosion severity is similar to the discussion for minibeams.

FIGURE 42 Typical corroding bars at the end of testing.

4 PLANS FOR IMPLEMENTATION

The PI recommends that field trials and additional testing should be performed. The developer of the TZD bars is ready to produce reinforcement that can be used in a highway structure application or for fabrication of larger laboratory specimens. Since the start of this program, the TZD developer has identified improved organic coating systems as well as other means of passivating the bar surface such as conventional chromates or some proprietary products. The longest bars that can be currently produced are 40 ft.; however, it is feasible to build an oven to treat 60 ft. bars.

The cracked beam tests showed superior performance to HDG bars. With a thinner coating, TZD reinforcement would be cost-competitive and reduce the reinforcing bar weight per foot. In addition, unlike the HDG bars, the TZD bars demonstrated a similar negative shift in corrosion potential at corrosion initiation as BB. This improves the ability to nondestructively monitor performance over time using potential measurements, simplifying the analysis required by DOTs.

Another advantage is that the TZD bars appear to improve bond and reduce the depth of migration of chloride through a crack. At the same loading of BB, the performance improvement might be greater in the field than that seen in the laboratory.

If a state decides to conduct field trials, the PI suggests that initial deployment could be as reinforcement used in barriers or as deck reinforcement for rural bridges with low traffic where there is a benefit for corrosion protection. The chloride ion concentration corrosion threshold value appears to be greater than 1,400 ppm by mass of concrete (8,200 ppm/0.82% cement). In several applications, using low permeability and reinforcing bar cover, such that chloride threshold levels are not exceeded, could result in 75+-year design service lives obtainable at a lower cost that using stainless steel bars.

5 CONCLUSIONS

The testing program evaluated several commercially available corrosion-resistant reinforcing bars as well as the TZD and TZE experimental products. All of the bars showed an improvement over BB in the testing.

The cracked beam tests using a better quality concrete and reinforcing bar cover provided a more realistic test environment than the lower cover U-bend specimens but was an accelerated test. In addition, it was learned after producing the U-bend specimens that the bars should have been bent beyond 180°, according to the bend test requirements in ASTM A615, so that they could spring back to 180 degrees and thus have lower stress. Since an intermetallic zinc coating is more brittle than pure zinc this would have helped to improve performance. The bars in the minibeams were under stress to keep the cracks open. That was a more realistic stress, though potentially still higher for TZD as it appeared to have improved bond, which could reduce in lower crack openings versus the control at the same load. The overall corrosion susceptibility in the cracked beam test evaluating both the top and bottom bars was:

$$BB > HDG > X35 > TZE \approx TZD > ECR > SS$$

Though this was an accelerated test, it was not accelerated enough for the ECR, which, if defects are low, fails more from an aging effect of the coating. The light abrasion used was not severe enough, and that would be something to address in future studies with ECR. The TZD and HDG coatings will not damage under most conceivable construction conditions so a more realistic means of damaging the ECR is needed, or tests need to be conducted over longer periods of time.

The order of corrosion flips between the HDG and TZD in the U-bend testing. This is most likely due to the fast ingress of chloride, which exceeded threshold levels soon after passivation occurred, and chloride values at the reinforcing bar were equivalent to or higher than at the reinforcement level in the minibeams. Even with the cracks in the beam, the bar away from the crack could passivate, and apparently there was some passivation in the cracks, which helped the TZD and HDG specimens. The HDG did better as it had a thicker zinc coating and a commercial chromate passivation treatment.

The advantages to considering the use of TZD and TZE are:

- Equal to lower cost than HDG at better performance
- Improved bond potentially reducing crack widths and migration of chloride to bottom mat bars under surface cracks
- Improved welding
- Low application temperature that could allow it to be applied to higher strength reinforcing bars to increase bond strength.

The cracked beam test as used here is a good test to evaluate the corrosion performance. The cracks were flexure-induced and coupled with periodic fatigue loading, more representative of field exposures. Of interest was that the

chloride concentration decreased deeper into the cracks, indicating that cracks in concrete where the reinforcing bars have not gone beyond their yield stress will taper. However, as was seen in this study, monitoring of just the macrocell currents is insufficient to identify actual performance. This test could be developed into an AASHTO test method to evaluate both reinforcing bars and other corrosion protection systems.

The U-bend tests could be a useful screening test with a few modifications. One change would be not to overly stress the bars or just use a straight bar. Then the chloride content could be determined away from the bar when corrosion initiates, and the test could still continue. This too could be developed into an AASHTO test method.

6 INVESTIGATOR PROFILES

Dr. NEAL BERKE, FACI, FASTM, FNACE

The principal investigator, Dr. Neal S. Berke, FACI, FASTM, FNACE, has more than 40 years of working in the field of corrosion with more than 30 years of experience with the corrosion of steel in concrete. He has more than 40 U.S. patents related to concrete durability and corrosion of steel in concrete. He has developed several ASTM standards and has participated on several in ACI and NACE. In addition to being a fellow in ACI, ASTM, and NACE he has received the ASTM Francis L. LaQue Aw**a**rd, ASTM Frank E. Richart Award, ACI Jean-Claude Roumain Innovation in Concrete Award, and several others recognizing his work in corrosion and concrete durability and technology.

RANJANI VIJAYAKUMAR

Co-investigator, Ranjani Vijayakumar, graduated from University of Illinois, Urbana–Champaign with a Master's of Science degree in Civil Engineering and joined Tourney Consulting Group, LLC in 2013. She has worked on various projects involving corrosion testing and concrete durability. She has a Cathodic Protection Technician Certification from NACE. She is a member of NACE.

7 GLOSSARY AND REFERENCES

7.1 GLOSSARY

Macrocell corrosion: the corrosion that occurs when the corrosion rate of a metal is increased by having it in contact with another metal. For concrete this usually refers to a bar in chloride contaminated concrete that is coupled to a bar in concrete with less chloride where the bar with less chloride causes the bar with more chloride to corrode faster, and its corrosion rate remains low.

Macrocell current: the current measured as the voltage drop across a resistor that connects the reinforcing bar closest to the surface to bars near the bottom of the specimen. It is a measurement of the macrocell corrosion rate. When integrated over time it gives the macrocell corrosion.

Polarization resistance: a nondestructive means of measuring the corrosion rate of a metal by slightly varying its voltage (potential) versus a stable material (reference electrode) and measuring the current needed to change the voltage. The slope of the voltage versus current curve at zero current is the polarization resistance, R_p.

7.2 REFERENCES

1. O'Reilly, M., D. Darwin, J. Browning, and C.E. Locke, Jr., *Evaluation of Multiple Corrosion Protection Systems for Reinforced Concrete Bridge Decks*, Report FHWA-KS-11-1, 2010, 567 pp.

2. Darwin, D., J. Browning, C.E. Locke, Jr., and T.V. Nguyen, *Multiple Corrosion Protection Systems for Reinforced Concrete Bridge Components*, Report FHWA-HRT-07-043, 2007, 92 pp.

3. McDonald, D.B., D.W. Pfeiffer, and M.R. Sherman, *Corrosion Evaluation of Epoxy-Coated, Metallic-clad and Solid Metallic Reinforcing Bars in Concrete*, Report FHWA-RD-98-153, 1998, 13 pp.

4. Ohno, Y., S. Praparntanatorn, and K. Suzuki, "Influence of Cracking and Water Cement Ratio on Macrocell Corrosion of Steel in Concretein," In *Corrosion of Reinforcement in Concrete Construction*, C.L. Page, P.B. Bamforth, and J.W. Figg Eds., Society of Chemical Industry, Cambridge, U.K., July 1996, pp. 24–32.

5. Schiessel, P., “Effectiveness and Harmlessness of Calcium Nitrite as a Corrosion Inhibitorin,” RILEM International Symposium on the Role of Admixtures in High Performance Concrete, Monterrey, Mexico, 1999.

6. Berke, N.S., M.P. Dallaire, and M.C. Hicks, “Corrosion of Steel in Cracked Concretein,” *Corrosion*, Vol. 49, No. 11, Nov. 1993, pp. 934–943.

7. Berke, N.S., D.F. Shen, and K.M. Sundberg, “Comparison of the Polarization Resistance Technique to the Macrocell Corrosion Technique,” In *Corrosion Rates of Steel in Concrete*, ASTM STP 1065, N.S. Berke, V. Chaker, and D. Whiting, Eds., ASTM, Philadelphia, Pa., 1990, pp. 38–51.

8. Berke, N.S., D.F. Shen, and K.M. Sundberg, “Comparison of Current Interruption and Electrochemical Impedance Techniques in the Determination of the Corrosion Rates of Steel in Concrete,” In *The Measurement and Correction of Electrolyte Resistance in Electrochemical Tests*, ASTM STP 1056, L.L. Scribner and S.R. Taylor, Eds., ASTM, Philadelphia, Pa., 1990, pp. 191–201.

9. Berke, N.S., “The Effects of Calcium Nitrite and Mix Design on the Corrosion Resistance of Steel in Concrete (Part 1),” *Corrosion 85*, National Association of Corrosion Engineers, Houston, Paper No. 273, 1985.

APPENDIX A

A1 COMPOSITION OF STEEL USED

Steel	Yield (ksi)	Tensile (ksi)	Elong. % (in 8")	Composition (Wt. %) Balance is Fe														
				C	Ni	Mn	Cr	P	Mo	S	V	Si	Cb	Cu	Sn	N	B	C.E.
BB/TZD	63.8	102.9	13.0	0.40	0.14	1.23	0.17	0.014	0.033	0.034	0.006	0.23	0.003	0.32				0.64
HDG/ECR	67.9	96.1	15.0	0.28	0.16	1.12	0.20	0.017	0.055	0.032	0.045	0.22	0.002	0.34				0.50
A 1035	134.0	174.0	9.5	0.12	0.10	0.69	9.50	0.009	0.020	0.015	0.019	0.34		0.16	0.008	0.01		1.19
S2304	101.0	123.0	23.0	0.02	3.58	1.71	22.76	0.020	0.290	0.001		0.45				0.18	0.002	

A2 REINFORCING BARS

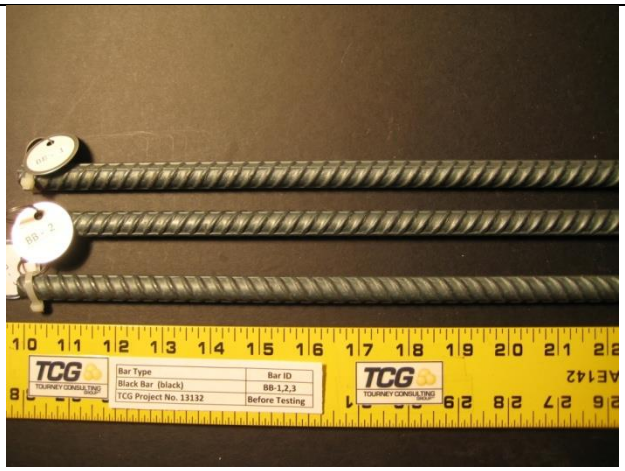

Black Bars

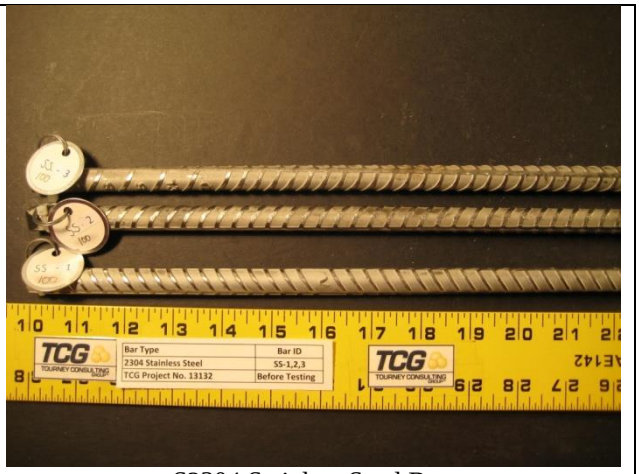

S2304 Stainless Steel Bars

A 1035 Bars

Hot-Dipped Galvanized (HDG) Bars

Epoxy-Coated Bars

Thermal Zinc Diffusion (TZD) Bars